Article

SOURCE DATA | TRANSPARENT PROCESS | OPEN ACCESS

THE EMBO JOURNAL

Cryo-EM structure of the chain-elongating E3 ubiquitin ligase UBR5

Zuzana Hodáková[1,*,†], Irina Grishkovskaya[1,†], Hanna L Brunner[1,2], Derek L Bolhuis[3], Katarina Belačić[1], Alexander Schleiffer[1], Harald Kotisch[1], Nicholas G Brown[4,**] & David Haselbach[1,***]

Abstract

UBR5 is a nuclear E3 ligase that ubiquitinates a vast range of substrates for proteasomal degradation. This HECT domain-containing ubiquitin ligase has recently been identified as an important regulator of oncogenes, e.g., MYC, but little is known about its structure or mechanisms of substrate engagement and ubiquitination. Here, we present the cryo-EM structure of human UBR5, revealing an α-solenoid scaffold with numerous protein–protein interacting motifs, assembled into an antiparallel dimer that adopts further oligomeric states. Using cryo-EM processing tools, we observe the dynamic nature of the UBR5 catalytic domain, which we postulate is important for its enzymatic activity. We characterise the proteasomal nuclear import factor AKIRIN2 as an interacting protein and propose UBR5 as an efficient ubiquitin chain elongator. This preference for ubiquitinated substrates and several distinct domains for protein–protein interactions may explain how UBR5 is linked to several different signalling pathways and cancers. Together, our data expand on the limited knowledge of the structure and function of HECT E3 ligases.

Keywords cryo-EM; HECT; Ubiquitin-Proteasome system; UBR5
Subject Categories Post-translational Modifications & Proteolysis; Structural Biology
DOI 10.15252/embj.2022113348 | Received 20 December 2022 | Revised 30 May 2023 | Accepted 14 June 2023 | Published online 6 July 2023
The EMBO Journal (2023) 42: e113348

Introduction

Ubiquitination is a fundamental post-translational modification that plays a role in the majority of signalling cascades in the cell. It is catalysed by the E1-E2-E3 enzyme cascade where, through specificity conferred largely by the E3 ligase, desired substrates are ubiquitinated. Ubiquitination is well-known for its role in protein degradation, where targeted substrates are marked for proteolysis by the proteasome (Komander & Rape, 2012). In this manner, important signalling proteins, such as transcription factors and nuclear receptors, can be swiftly turned over (de Almeida *et al*, 2021).

E3 ligases are separated into two major classes, divided by their mechanism of action. HECT (Homologous to the E6-AP Carboxyl Terminus) E3 ligases typically function as single polypeptide enzymes, with substrate recruitment and catalytic modules embedded within their structure (Lorenz, 2018). In contrast, the largest and most characterised E3 ligase family, RING (really interesting new gene) family, form multiprotein assemblies. For example, substrate recruitment by the Skp1-Cullin1-F-box (SCF) E3 ligase complex occurs through one of the 70 available F-box proteins and requires coordination with several accessory proteins to accomplish ubiquitination (Harper & Schulman, 2021). Similarly, the 19 polypeptide Anaphase-Promoting Complex/Cyclosome (APC/C) adopts distinct conformations of its catalytic module to accomplish polyubiquitination (Brown *et al*, 2016). Instead, a large structural heterogeneity exists within the single chain HECT E3 ligases, which are predicted to contain numerous distinct protein-binding modules, possibly to ubiquitinate a wide range of substrates without the need for adaptor proteins.

One of the largest HECT E3s is UBR5 (also known as EDD or N-recognin), a nuclear protein containing 2,799 residues in humans. UBR5 was identified as a tumour suppressor gene in *Drosophila* (Mansfield *et al*, 1994) and is embryonic lethal upon knockout (Saunders *et al*, 2004). In the past decade, a wealth of new data has ascribed a range of substrates and functions attributed to UBR5. For example, UBR5-mediated ubiquitination regulates key events like mitotic progression (Scialpi *et al*, 2015; Kaisari *et al*, 2022), DNA replication (Cipolla *et al*, 2019), transcription and DNA damage response (DDR; Henderson *et al*, 2006; Gudjonsson *et al*, 2012; Zhang *et al*, 2014; de Vivo *et al*, 2019), or NF–κB immune signalling via the nuclear factor Akirin (Cammarata-Mouchtouris *et al*, 2020), among others (Shearer *et al*, 2015).

1 Research Institute of Molecular Pathology (IMP), ViennaBioCenter (VBC), Vienna, Austria
2 Vienna BioCenter PhD Program, Doctoral School of the University of Vienna and Medical University of Vienna, Vienna, Austria
3 Department of Biochemistry and Biophysics and Lineberger Comprehensive Cancer Center, University of North Carolina School of Medicine, Chapel Hill, NC, USA
4 Department of Pharmacology and Lineberger Comprehensive Cancer Center, University of North Carolina School of Medicine, Chapel Hill, NC, USA
*Corresponding author. Tel: +431797303009; E-mail: zuzana.hodakova@imp.ac.at
**Corresponding author. Tel: +19199661235; E-mail: nbrown1@med.unc.edu
***Corresponding author. Tel: +431797303009; E-mail: david.haselbach@imp.ac.at
†These authors contributed equally to this work

UBR5's vast substrate selection is further reflected in its implications in several cancers, including breast (Liao *et al*, 2017), ovarian (Clancy *et al*, 2003), pancreatic (Li *et al*, 2021), colorectal cancers (Wang *et al*, 2017) or mantle cell lymphoma (Meissner *et al*, 2013). Tumorigenesis can stem from the loss of UBR5 and the subsequent deregulation of important cellular processes such as the DDR, or through direct effects on cellular levels of multiple proto-oncogenes, including p53 (Ling & Lin, 2011) or β-catenin (Flack *et al*, 2017). Recently, data from our group and others described the importance of UBR5 in cell growth via MYC degradation (Qiao *et al*, 2020; Schukur *et al*, 2020; de Almeida *et al*, 2021). In contrast, UBR5 can also influence tumorigenesis with its oncogene-like functions, e.g., enhancing tumour growth through inhibition of the cytotoxic T-cell response or modulating tumour microenvironments through immunosuppression (Song *et al*, 2020a,b).

The ability of UBR5 to recognise and ubiquitinate a multitude of substrates, resulting in tumour-suppressing and/or oncogene-like functional versatility, is poorly understood. Current structural information is limited to crystal structures of isolated domains (Kozlov *et al*, 2007; Matta-Camacho *et al*, 2012; Muñoz-Escobar *et al*, 2015), leaving the majority of UBR5 structurally uncharacterised. The UBR5 C-terminus contains the HECT catalytic domain, the only conserved feature across all ~28 HECT-type E3 ligases (Lorenz, 2018). While previous studies on isolated HECT domains explain crucial steps of ubiquitin transfer (Kamadurai *et al*, 2009, 2013; Maspero *et al*, 2011, 2013), resolving the first full-length structure of a HECT-type E3 ligase, HUWE1, revealed the importance of its complex architecture in substrate engagement in relation to ubiquitin transfer (Grabarczyk *et al*, 2021; Hunkeler *et al*, 2021). Yet, outside of the HECT domain, these enzymes are considerably different in sequence. Therefore, additional structural and biochemical information is needed to understand the polyubiquitination mechanism of UBR5 and HECT E3s in general.

To determine the interplay and spatial arrangement between the catalytic HECT domain and predicted protein-interacting domains of UBR5, we solved the structure of full-length human UBR5 using electron-cryo microscopy (cryo-EM). We uncovered tetrameric and larger oligomeric assemblies of UBR5, with homodimers as a minimal building block. The central feature of each UBR5 protomer is its large α-solenoid helical scaffold, decorated with numerous putative protein-binding domains, aiding in E2-ubiquitin transfer, oligomerisation and catalysis. We further uncover AKIRIN2 as a substrate and observe a preference of UBR5 to extend ubiquitin chains from a pre-ubiquitinated substrate, suggesting UBR5 functions primarily as a chain-elongating enzyme. We observe oligomerisation is not a key feature governing ubiquitination activity in our assays, and propose it might be important for substrate recruitment. Taken together, our structural and biochemical information begins to unravel the versatility of UBR5 and HECT E3 ligases in substrate choice and function.

Results

UBR5 dimer is the building block for oligomerisation

We expressed two full-length UBR5 constructs in HEK293T cells; an N- and C-terminally tagged construct, hereafter referred to as UBR5, and UBR5 with a native C-terminus, hereafter referred to as UBR5^{wt}, to avoid potential changes to UBR5's activity by modifying its C-terminus (Kim & Huibregtse, 2009). In both cases, purification by size exclusion chromatography (SEC) revealed two elution peaks (Fig EV1A). We assessed the peak heterogeneity using mass photometry (MP), a method to measure the mass distribution of a given sample (Sonn-Segev *et al*, 2020). We found a range of oligomers was formed in a repeating order of two. Monomeric UBR5 was not detected (Figs 1A and B and EV1B). The oligomers remained stable across a range of buffer conditions and possibly adopted higher oligomers with increased temperature (Fig EV1C). These results suggested that UBR5 forms stable dimers as the building block and functional unit of all oligomers.

We selected the most homogeneous, predominantly tetrameric UBR5 sample from the second SEC elution peak for structural analysis using single-particle cryo-EM. 2D classification and subsequent processing revealed UBR5 forms a ring-shaped assembly with a 215 Å diameter and a large central cavity (Fig 1C and D). Docking in four copies of a monomeric UBR5 structure predicted by AlphaFold2 into our cryo-EM map fully occupied the density (Appendix Fig S1A), consistent with our MP measurements. Notably, our structure predictions of UBR5 dimers or tetramers using AlphaFold2 did not predict sensible assemblies (Appendix Fig S1B).

Our initial cryo-EM dataset suffered from preferred particle orientation to confidently build an atomic model. We therefore collected and merged several UBR5 datasets, which resulted in a higher map isotropy (Appendix Fig S2). Additionally, we observed conformational flexibility between two sides of the tetrameric ring, and global refinements converging with only one side of the map resolving well. To cope with this flexibility, we performed local refinements with a half-map mask. This approach allowed us to obtain a 3 Å cryo-EM map of the UBR5 homodimer (Fig 1E).

Dimerisation and tetramerisation interfaces are formed by distinct motifs

Using the AlphaFold2-predicted UBR5 model as a template for model building, we were able to confidently model the UBR5 homodimer, characterise the dimerisation interface and assign densities of several protein-binding domains of UBR5 (Figs 1F–H and EV2A). The central feature of the monomer is a 100 Å long α-helical solenoid between the N- and C-termini of UBR5, formed by armadillo and HEAT repeats.

The most striking feature of our cryo-EM density was the elegant assembly of UBR5 into an antiparallel homodimer. The dimerisation interface is mediated by a single helix (residues 1,912–1,931) of each protomer, protruding from one solenoid into a pocket of the opposite protomer (Fig 2A). The dimerisation helix consists of a hydrophobic core flanked by several charged residues accommodated within a hydrophobic cavity of the opposite protomer's pocket (Fig 2B). Similar to the helix, the pocket is flanked with several charged residues, which form salt bridges with the dimerisation helix. Residues forming this interaction are highly conserved across multiple species, ranging from *C. elegans* to humans (Appendix Fig S3-Dark green stars).

To confirm the role of the helix in UBR5 dimerisation, we expressed mutants aimed at disrupting this interface using insect cell expression system (represented as (i) with each construct). We first characterised and compared full-length proteins (UBR5^{wt} and UBR5$^{wt(i)}$) using SEC, ThermoFluor and MP to confirm their

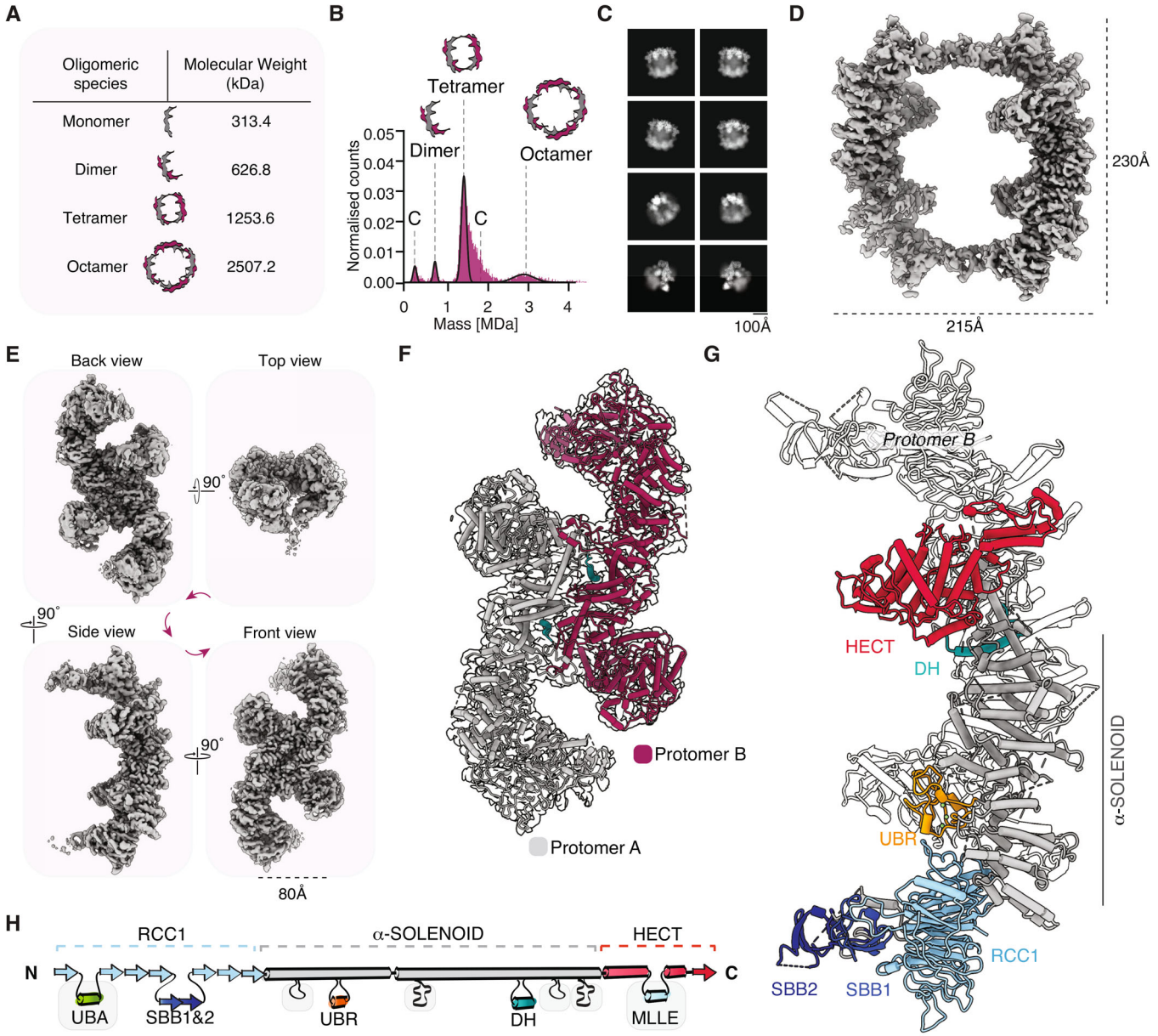

Figure 1. Cryo-EM characterisation of dimeric and tetrameric UBR5 assemblies.

A Expected molecular weights of UBR5 oligomers.

B Mass distribution and oligomeric states of UBR5 sample used for cryo-EM, measured using MP. Contaminant peaks and shoulders are annotated with "C". Full mass measurements are listed in Dataset EV1.

C A representative selection of 2D classes of UBR5.

D Single particle cryo-EM reconstruction of the tetrameric UBR5.

E High-resolution cryo-EM reconstruction of the UBR5 dimer.

F Protomer assembly in a UBR5 dimer.

G Atomic model of UBR5 resolved in this study.

H Schematic linear representation of UBR5 domains and motifs described in this study, colour-coded and annotated as in (G). UBA, Ubiquitin associated domain; RCC1, Regulator of chromosome condensation 1; SBB, small β barrel; UBR, UBR box; DH, dimerisation helix; HECT, Homologous to the E6AP Carboxyl Terminus; MLLE, Made-moiselle/PABC. Unresolved domains and loops are represented in grey boxes.

oligomerisation properties and stability (Appendix Fig S1C and D, Fig EV1D). We subsequently purified and characterised two mutants; a deletion of the entire dimerisation helix (residues 1,912–1,931), UBR5$^{\Delta DH(i)}$ and a UBR5 mutant with three charge-reversing point mutations of the key residues of this interface, UBR5$^{DHmutant(i)}$; 1914 (R > D), 1926 (R > D) and 1931 (E > R). Both mutants displayed a change in their oligomeric properties, with monomers becoming the predominant species (Fig 2C). We still observed a

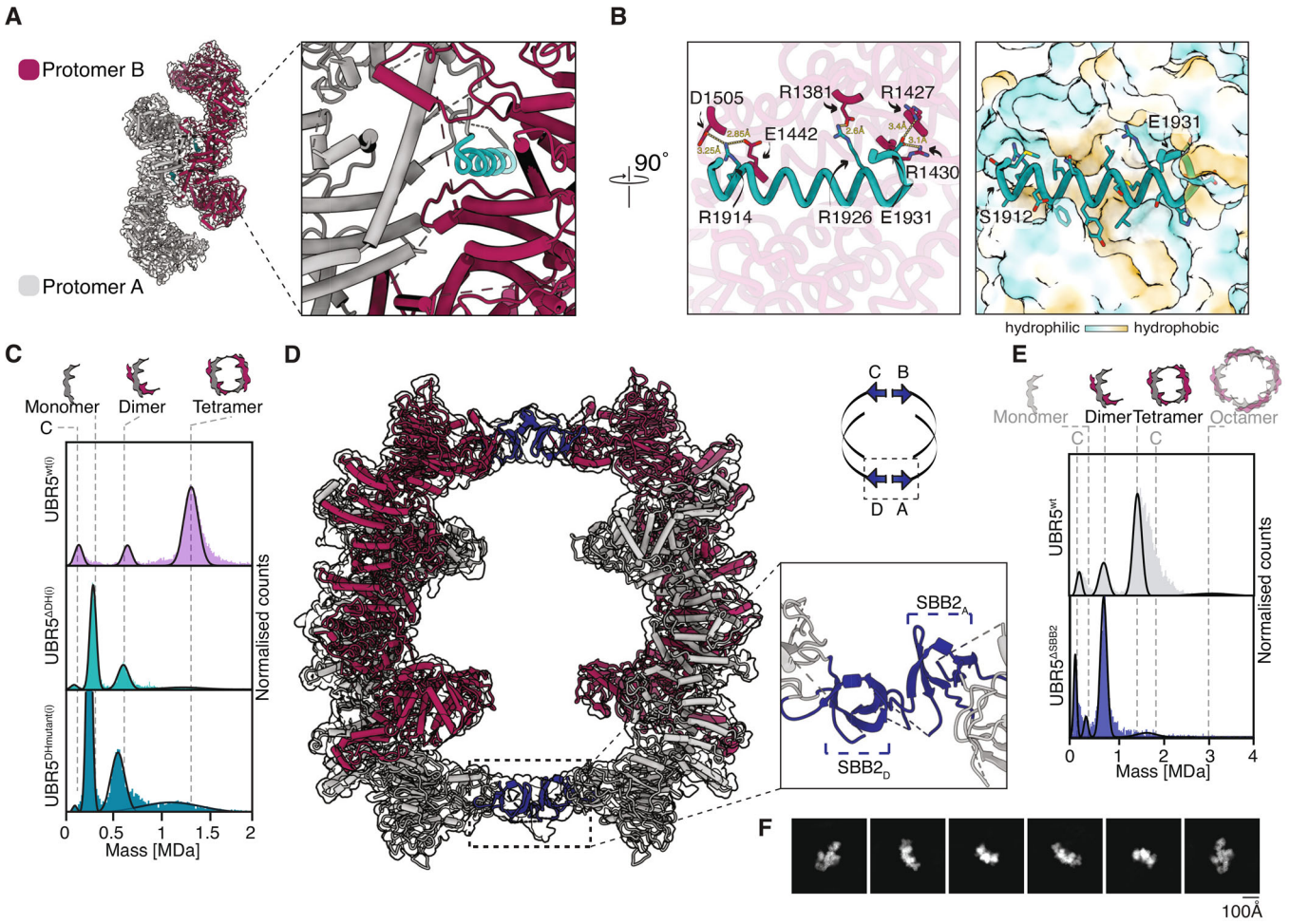

Figure 2. Substrate-recognition and tetramerisation motifs of UBR5.

A Enhanced view of the dimerisation interface between two UBR5 protomers in one dimer unit. Dimerisation helix of protomer A is represented in teal.

B Molecular details of the dimerisation interface. The left box represents the charged interactions of this interface, colour coded as in (A). Key residues of protomer B's pocket are further highlighted in magenta. The right box visualises the hydrophobic cavity of the dimerisation pocket with the dimerisation helix (in teal).

C Mass distribution and oligomeric states adopted by full-length and dimerisation-impaired mutants of UBR5. Y-axes were normalised equally to a scale of 0–0.05 of normalised counts.

D Protomer assembly in the tetrameric UBR5 cryo-EM reconstruction and an enhanced view of the tetramerisation interface. The protomer arrangement is further visualised in the simple schematic; highlighted domains in dark blue represent the tetramerisation interface (SBB2 domains).

E Mass distributions of full-length UBR5 and a tetramerisation-impaired mutant. Y-axes were normalised equally to a scale of 0–0.05 of normalised counts.

F Representative 2D classes of tetramerisation-impaired mutant UBR5$^{\Delta SBB2}$.

small proportion of dimeric and tetrameric species, which we attribute to residual interactions occurring even with constructs designed to disrupt the interface completely, possibly because we did not resolve the entire interface in our cryo-EM maps.

Another striking finding was the complex spatial arrangement of putative substrate engagement motifs across the entire length of UBR5 (Fig 1G and H). The N-terminus revealed an elaborate assembly of four domains: the absolute N-terminus consists of a 7-bladed β-propeller Regulator of Chromosome Condensation 1 (RCC1) domain, with two discontinuities in the form of three accessory domains. We observed smaller globular densities in close proximity to the RCC1 domain, which we located as an insertion to the 4th blade of the RCC1 domain. Due to resolution limitations in our cryo-EM reconstructions, we could not build the corresponding part of the model outright. Therefore, we assigned the relative positions with AlphaFold2-predicted domains, which occupy the density with good agreement. Their predicted secondary structure, composed of a five β-strand assembly, is reminiscent of small β-barrels (SBBs; Youkharibache *et al*, 2019). Thus, we annotated these domains as SBB1 and SBB2, two motifs which are linked in tandem (Fig EV2-iii).

Small β-barrel domains were often found to facilitate oligomerisation via β strand hydrogen bonding (Youkharibache *et al*, 2019). To identify if these motifs form the tetramerisation interface of UBR5, we performed extended 3D classification of the tetramer to obtain a more rigid density. We could not assign the atomic

coordinates of these domains due to low resolution, but we confidently docked in two UBR5 dimers. This revealed that this assembly is indeed facilitated by SBB2 domains of two opposite dimers (Fig 2D). We confirmed the role of SBB2 domains in UBR5 tetramerisation by expressing a UBR5 mutant with an SBB2 domain deletion ($UBR5^{\Delta SBB2}$) and analysing its oligomeric state using MP. This revealed an almost exclusively dimeric assembly of UBR5 (Fig 2E). We observed a small peak with a molecular weight of a tetramer. This peak is of considerably lower abundance than the dimeric peak, but it cannot be excluded that UBR5 dimers display weak binding properties to each other even in the absence of SBB domains. We further subjected $UBR5^{\Delta SBB2}$ to cryo-EM analysis. 2D classification of this mutant revealed an exclusive dimeric assembly, further confirming the role of SBB2 domains in contacts between two dimers (Fig 2F).

We additionally performed 3D variability analysis (3DVA; Punjani & Fleet, 2021), which visualised a dynamic movement between two opposing dimers (Movie EV1). These dynamics appeared to stem from the SBB2 domain contacts. The interactions could be transient, allowing UBR5 to oligomerise into higher multimers.

UBR5 homodimers are decorated with protein-interacting domains

Aside from their tetramerisation function, the protein-interacting motifs of the UBR5 N-terminus could also serve as protein-recruiting platforms. We resolved the prominent N-terminal RCC1 domain, which showed a near-identical conformation to the chromatin-binding RCC1 protein (Renault *et al*, 2001; Fig EV2A-ii). RCC1 domains are also found in other HECT-type E3 ligases, such as in the HERC family, where they form numerous interactions, for example, with other E3 ligases (García-Cano *et al*, 2019). The SBB insertions in this domain could also play a role in substrate recruitment. Common domains of the SBB fold type include the SH or OB folds, which are involved in various RNA-processing steps (Kambach *et al*, 1999). It is plausible that aside from their contribution to oligomerisation, the SBB domains of UBR5 also interact with RNA-binding proteins (Youkharibache *et al*, 2019). Another discontinuity inserted between the first and second blade of the RCC1 domain is the ubiquitin-associated (UBA) domain, previously described to interact with monoubiquitin and polyubiquitin chains (Kozlov *et al*, 2007). UBA is tethered to RCC1 via long flexible loops, a likely explanation for why we do not resolve the UBA domain in our cryo-EM maps. Its position thus remains speculative (Fig EV2A-i).

A key feature placing UBR5 in the UBR family of E3 ligases/N-recognins, is the UBR box, embedded within the fourth armadillo repeat (Varshavsky, 2011). Due to the overall folding of UBR5, the box is positioned right above the RCC1 domain, albeit separated by several helical turns of the scaffold. The UBR box is a conserved zinc-finger-like substrate recognition domain of all members of the UBR family (Kim *et al*, 2021). Alignments of UBR2 and UBR5 UBR boxes showed high conservation across the domain. We docked in three Zinc atoms from the UBR2 structure into our UBR5 model. The zinc atoms, coordinated by two histidines and eight cysteines in UBR5, stabilise the tertiary fold of this domain (Choi *et al*, 2010; Matta-Camacho *et al*, 2010; Fig EV2A-v and B).

Similar to UBR1, 2 and 4, UBR5 was reported to bind type-I Arg/N-degrons, which contain positively charged terminal residue and a hydrophobic penultimate residue (Tasaki *et al*, 2009). These two residues bind a negatively charged pocket and a secondary hydrophobic pocket of the UBR boxes, respectively (Matta-Camacho *et al*, 2010; Muñoz-Escobar *et al*, 2017). Comparison of the UBR2 and UBR5 UBR box sequence and surface charges suggest the negatively charged pocket in UBR5 is less prominent, formed by two acidic residues (D1233 and E1236) instead of three (Fig EV2B and C). The third is swapped for a hydrophobic leucine (L1202), possibly extending the hydrophobic pocket for the penultimate degron residue binding. This amino acid composition of UBR5 UBR boxes is conserved across multiple species (Appendix Fig S3, underlined in orange). These changes in the UBR box of UBR5 could have an impact on its degron selection and influence its broad specificity (Tasaki *et al*, 2009).

Towards the C-terminus of the enzyme are the catalytic HECT domain and the protein interacting motif MLLE, also known as PABC (Homologous to the C-terminal region of poly-adenylation binding protein). Contrary to initial annotations (Deo *et al*, 2001), AlphaFold2 predicted UBR5 structure suggested this domain is an insertion in the HECT domain, separated with 40-amino acid long unstructured linkers on each side. Whilst we cannot resolve this domain due to its flexible nature, we could partially build the linkers which connect MLLE to the HECT domain, showing they are an extension of the N-lobe of the HECT domain (Fig EV2A-iv).

UBR5 is an efficient ubiquitin chain elongator

Our cryo-EM structure revealed numerous modules that could play a role in substrate engagement as well as ligase activity. To decipher the mode of ubiquitination of UBR5, we first focused on characterising the ubiquitination activity of full-length $UBR5^{wt}$. Previous reports suggest that the homologue of UBR5 in *D. melanogaster*, Hyd, ubiquitinates Akirin to influence NF–κB signalling (Cammarata-Mouchtouris *et al*, 2020). We have identified AKIRIN2, the human ortholog of Akirin, as a key regulator of MYC via facilitating the nuclear import of the proteasome (de Almeida *et al*, 2021). Aside from AKIRIN2, our screen also identified UBR5 as one of the key E3 ligases governing MYC turnover. We therefore hypothesised whether the interaction between UBR5 and AKIRIN2 is also found in higher eukaryotes.

We performed protein complex reconstitutions and ubiquitination assays using AKIRIN2 expressed as a recombinant fusion to GFP (^{GFP}AKIRIN2) and two control substrates, C-terminally FAM-labelled SECURIN ($SECURIN^{FAM}$) and GFP (Figs 3A and EV3A). We chose SECURIN because it is similar in length and secondary structure to AKIRIN2. We first tested whether ^{GFP}AKIRIN2 binds UBR5 using sucrose gradients. We observed that ^{GFP}AKIRIN2, but not the control substrates, co-sediment with UBR5, showing that they interact (Figs 3B and EV3B and E). Next, we asked whether UBR5 can ubiquitinate ^{GFP}AKIRIN2. We identified UBCH5B as a suitable E2 for UBR5 using a commercially available E2 screening kit (Appendix Fig S1E). Subsequently, we performed ubiquitination assays of ^{GFP}AKIRIN2, $SECURIN^{FAM}$ and GFP. Unexpectedly, substrates were not ubiquitinated by UBR5, despite the pool of free ubiquitin being depleted (Figs 3C and EV3C).

Because ^{GFP}AKIRIN2 bound UBR5, we considered the inability of UBR5 to ubiquitinate ^{GFP}AKIRIN2 stems from poor ubiquitin chain-initiating properties of the enzyme. We consequently

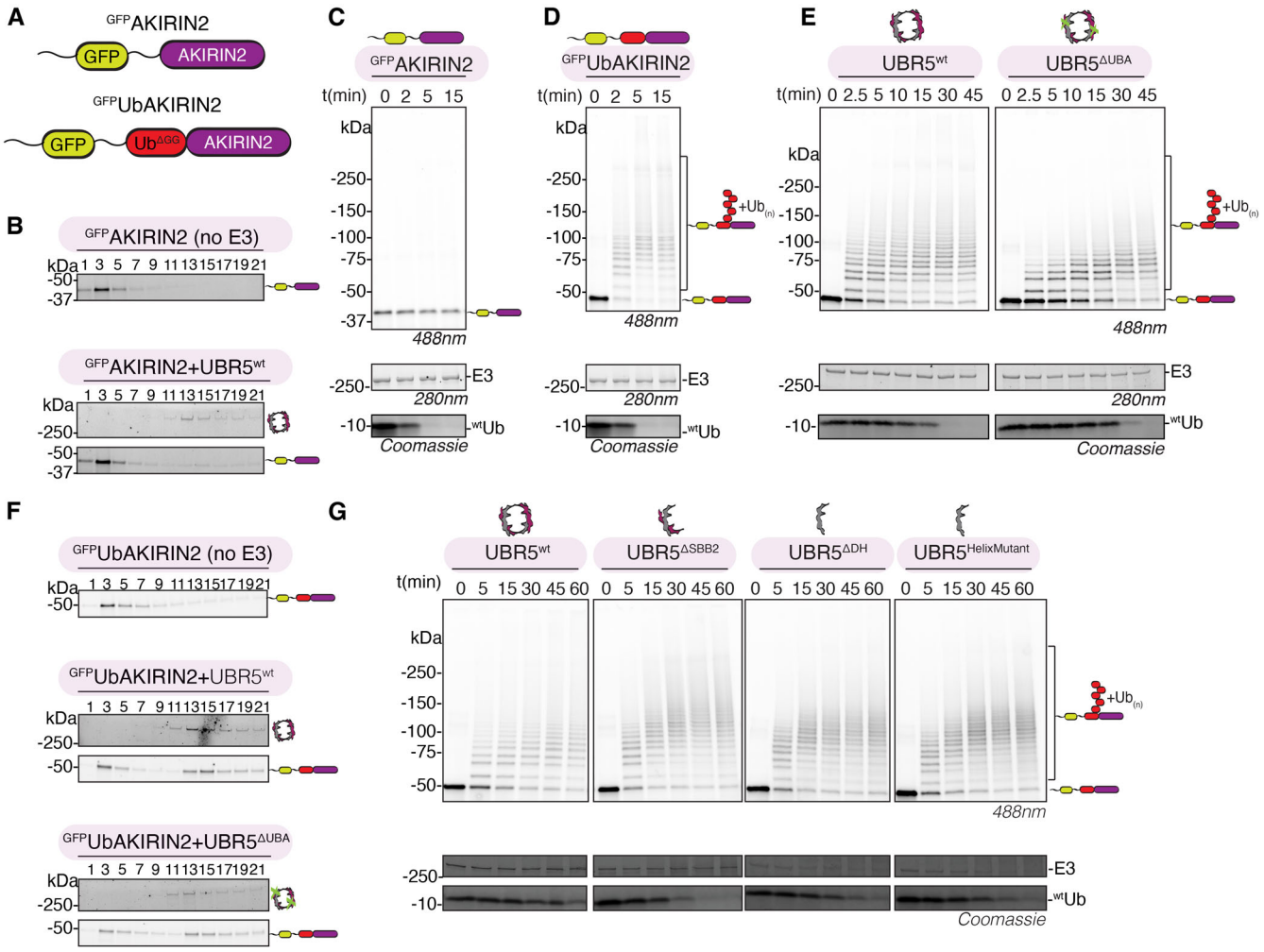

Figure 3. Substrate selection of and enzymatic activity of UBR5.

A A schematic representation of two AKIRIN2 constructs used in activity assays and complex reconstitutions.
B Sucrose gradient sedimentation profiles of ^{GFP}AKIRIN2 in the presence or absence of UBR5.
C Ubiquitination of ^{GFP}AKIRIN2.
D Ubiquitination of ^{GFP}UbAKIRIN2.
E Ubiquitination activity of wild-type and mutant UBR5$^{\Delta UBA}$ on ^{GFP}UbAKIRIN2 substrate.
F Sucrose gradient sedimentation profiles of ^{GFP}UbAKIRIN2 in the absence (upper panel) or in the presence of UBR5^{wt} (middle panel), and UBR5$^{\Delta UBA}$ (lower panel).
G Ubiquitination activity of wild-type and oligomerisation-defective mutants on ^{GFP}UbAKIRIN2.

Data information: Gels were imaged using fluorescent imaging (488 nm) to visualise the recombinant GFP tag, and stain-free imaging to visualise all proteins. Gels were subsequently stained using Coomassie staining to visualise ubiquitin levels. Gels of assays are a representative of at least three experimental replicates. Reactions in C and D were performed at 37°C. Reactions in E and G were performed at 25°C. The final concentration of E3 enzyme in C, D, E: 0.3 μM, in G: 0.2 μM.
Source data are available online for this figure.

anticipated UBR5 might be effective as a chain elongator with the pre-requisite of substrates carrying a ubiquitin modification. Therefore, we cloned the ubiquitin-coding sequence into our ^{GFP}AKIRIN2 construct as an N-terminal fusion to AKIRIN2 (^{GFP}UbAKIRIN2) or to SECURIN (UbSECURIN^{FAM}) to mimic substrate monoubiquitination (Figs 3A and EV3A), and tested both its binding and ubiquitination by UBR5. Using these primed substrates, we observed rapid growth of ubiquitin chains on both substrates (Figs 3D and EV3D). To further confirm the chain-elongating properties of UBR5 in the absence of substrate, we tested a Cy5-labelled ubiquitin with a deletion of the two C-terminal glycine residues (^{Cy5}UbΔGG). We used this mutant ubiquitin to obtain clear assay read-outs, as it can only serve as a ubiquitin acceptor. Indeed, UBR5 was able to form chains on the acceptor ^{Cy5}UbΔGG (Fig EV3G). Further mass spectrometry analysis of ubiquitinated ^{GFP}UbAKIRIN2 and ^{Cy5}UbΔGG demonstrated UBR5 is predominantly specific for K48-linked chains. Only a minor proportion of AKIRIN2 was ubiquitinated (Fig EV3H). Taken together, UBR5 efficiently elongated chains on substrates which pre-possessed a ubiquitin modification.

We thus wondered whether pre-ubiquitinated substrates also bind UBR5 better than non-ubiquitinated counterparts. We repeated sucrose gradient experiments, comparing the sedimentation profiles of ^{GFP}AKIRIN2 and ^{GFP}UbAKIRIN2. We observed a strong shift in the gradient when AKIRIN2 carried a ubiquitin modification (Fig 3F). In contrast, very little UbSECURIN^{FAM} formed a complex with UBR5 (Fig EV3F).

The UBA domain increases UBR5-dependent ubiquitination activity

Our findings that the primed substrate, ^{GFP}UbAKIRIN2, engages UBR5 stronger than its non-ubiquitinated counterpart, suggest an avidity mechanism of binding. Aside from the catalytic HECT domain, our sequence conservation analysis predicted only one additional ubiquitin-binding domain, the UBA domain, in agreement with previous reports that this domain binds ubiquitin (Kozlov *et al*, 2007; Appendix Fig S3). We therefore set out to test whether the UBA domain plays a role in ubiquitinated substrate engagement. We generated a UBA domain deletion mutant (UBR5$^{\Delta UBA}$) based on the AlphaFold2-generated full-length UBR5 model and the available UBR5 UBA domain crystal structure (Kozlov *et al*, 2007). We hypothesised that if the UBA domain aids in ^{GFP}UbAKIRIN2 recruitment, its deletion will reduce the amount of complex formed by the ubiquitin interaction. Surprisingly, sucrose gradient experiments of full-length and UBR5$^{\Delta UBA}$ revealed that the interaction of ^{GFP}UbAKIRIN2 was unaffected (Fig 3F bottom panel). This result suggests that UBR5 possesses an unanticipated ubiquitin-binding site that is currently unknown.

Based on the above observations, we wondered whether the UBA domain plays a role in substrate ubiquitination rather than binding. We therefore subjected ^{GFP}UbAKIRIN2 to ubiquitination by UBR5$^{\Delta UBA}$ and UBR5^{wt}. In the early ubiquitination time points, UBR5$^{\Delta UBA}$ displayed a defect in the added ubiquitin chain length (Fig 3E). With longer time points, UBR5$^{\Delta UBA}$ built polyubiquitin chains and depleted the free-ubiquitin pool but at a significantly slower rate than UBR5^{wt}. To assess if the defect arises from lower local ubiquitin concentrations as a result of decreased E2 ~ Ub recruitment, we gradually increased the E2 concentration in our ubiquitination assays to try to overcome this defect. However, this increase only partially restored the ubiquitination capabilities of UBR5$^{\Delta UBA}$ compared with the wild type (Fig EV3I). We further confirmed the defect stems from its inability to engage with ubiquitin by mutating two key residues of the UBA domain, which, based on a previous study, bind ubiquitin grooves (UBR5$^{V196K,\ L224K}$; Fig EV2A-i; Kozlov *et al*, 2007). These results show that the function of the UBA domain is, in part, involved in E2 ~ Ub recruitment, but it may serve additional roles.

UBR5 oligomerisation is not required for ubiquitin chain elongation

The striking revelation that UBR5 assembles into dimers and tetramers prompted the question if these features regulate the ubiquitination activity of the enzyme. We therefore subjected all our oligomerisation mutants (UBR5$^{\Delta SBB2}$, UBR5$^{\Delta DH}$, UBR5^{HelixMutant}) to ubiquitination assays of ^{GFP}UbAKIRIN2 (Fig 3G). We observed a similar rate of ubiquitin depletion and substrate ubiquitination of wild-type and dimerisation-impaired UBR5 mutants. Interestingly, disrupting the tetramerisation interface seemed to subtly enhance the activity of UBR5. Oligomerisation of UBR5 thus does not appear to be a crucial factor for its intrinsic activity of ubiquitin chain elongation.

Interfaces mediating the HECT domain and UBR5 activity

Whilst substrate recruitment to UBR5 may occur through numerous protein surfaces, ubiquitin transfer occurs through one domain; the C-terminal HECT domain and its catalytic cysteine. Structurally, HECT domains have a conserved architecture composed of N- and C-lobes separated by a short flexible linker (Huang *et al*, 1999; Verdecia *et al*, 2003). HECT E3 ligases catalyse ubiquitin transfer in two steps: first, the N-lobe interacts with the ubiquitin-loaded E2, followed by ubiquitin transfer and thioester linkage formation between ubiquitin and the acceptor cysteine of the C-lobe. This is accompanied by a rotation between N and C lobes (Kamadurai *et al*, 2009, 2013; Maspero *et al*, 2013). HECT domain mobility is a key feature for its catalytic function.

Our UBR5 maps show the lowest local resolution (~5 Å) in the HECT domain, which is often suggestive of protein flexibility. Indeed, using 3DVA, we observed a movement of the HECT domain with respect to the rest of the protein (Movie EV2). We identified two states: in state 1, the HECT domain is positioned with its N lobe rotated upwards towards the RCC1 domain of the adjacent protomer. In the less abundant state of our dataset, state 2, the N-lobe rotates 30° away from RCC1 (Fig 4A and B). This rotation is also visible in the initial 2D classes from the entire dataset (Fig 4C). Aligning the Nedd4-Ubch5 structure into both states revealed that E2 engagement in state 1 would lead to a steric clash between the E2 enzyme and the RCC1 domain of the second protomer. However, in state 2, the 30° HECT domain rotation expands the cleft sufficiently to accommodate an E2 (Fig EV4A).

HECT domain mobility was also observed in the HUWE1 ligase, the only other reported HECT ligase with a solved full-length structure. In HUWE1, a hinge-like set of three helices connecting the solenoid body to the base of the N-lobe were found to influence its activity (Sander *et al*, 2017; Grabarczyk *et al*, 2021; Hunkeler *et al*, 2021). Our structure also revealed a three-helix bundle with similar key residues to HUWE1, forming the only continuous contact between the solenoid scaffold and the HECT domain (Figs 4D and EV4B). We could not further refine particles of state 2 to obtain more structural information on this domain, as the region appeared less resolved, suggesting more motion in state 2. Overall, the hinge position with respect to the HECT domain as well as its key residues, are reminiscent of HUWE1 and could thus serve similar, not fully understood, roles in HECT domain orientation.

Our structure further revealed a stretch of 25 amino acids extending from the α-solenoid between the lobes of the HECT domain before looping back (Fig 4E). We termed this region the plug loop, as it occludes the space between the N and C lobes. This loop does not precede the hinge or HECT domains in a linear sequence but rather is separated by almost 200 unstructured residues. To test whether this loop plays a crucial role in UBR5 activity, we generated a deletion mutant of the plug loop (UBR5$^{\Delta PL}$) and subjected it to activity assays. We observed rapid ubiquitin chain formation, showing it is not essential for UBR5 intrinsic activity

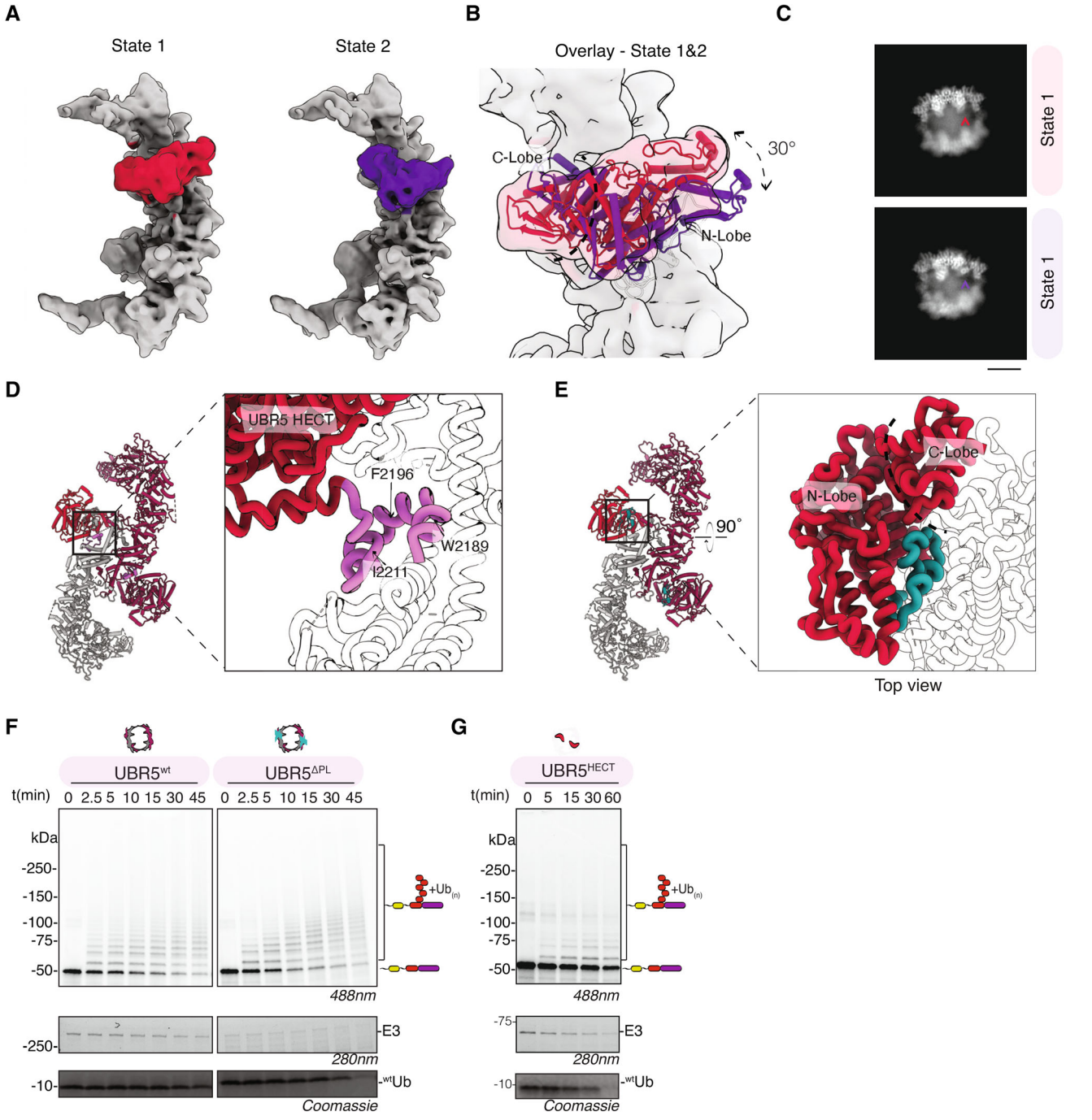

Figure 4. UBR5 HECT domain dynamics and structural features.

A Conformational states of the HECT domain identified using 3DVA.

B An overlay of the HECT domain models in either state described in (A), docked into the HECT domain density in State 1. The dashed double-sided arrow represents the shift observed between the two states.

C A selection of 2D classes from Fig 1C. Arrows point to the position of the HECT domain. Scale bar: 100 Å.

D The hinge domain of UBR5, shown in pink, connecting to the base of the HECT domain N lobe (in red). Residues, which could important for its function are annotated.

E Top view of the HECT domain (in red) and the plug loop in teal. The HECT domain lobes are separated by a dashed line and annotated.

F, G (F) Ubiquitination of ^{GFP}UbAKIRIN2 by UBR5 and UBR5$^{\Delta PL}$ and (G) isolated UBR5^{HECT}.

Data information: Gels were imaged as described in Fig 3. Gels of assays are a representative of at least two experimental replicates. Reactions in F were performed at 25°C and at 37°C in G. All the reactions were performed using a final concentration of 0.3 μM E3.
Source data are available online for this figure.

(Fig 4F). Instead, we noticed UBR5$^{\Delta PL}$ is unstable over time. Analysis of this mutant using ThermoFluor showed two melting temperatures, an unfolding behaviour suggestive of loss of protein folding co-operativity (Chari *et al*, 2015; Fig EV1C). This feature could therefore serve during protein assembly as a folding aid to the HECT domain, with future structural experiments necessary to elucidate its precise role. We additionally expressed and tested the activity of the isolated UBR5 HECT domain. We observed ubiquitination of ^{GFP}UbAKIRIN2 only after increasing the reaction temperature to 37°C (Fig 4G). The activity of the isolated HECT domain was significantly lower than for full-length UBR5 and all mutants. Moreover, this construct showed the lowest overall stability when measured with ThermoFluor, similar to results obtained for UBR5$^{\Delta PL}$. These results support the notion that substrate-recruiting regions of UBR5 are necessary for multiple steps in ubiquitin transfer.

Discussion

One of the largest HECT E3 ligases, UBR5, is an important regulator of multiple cellular processes with a wide array of substrates. Its nuclear localisation and implication in cancer biology make it an interesting target for cancer therapies. Our structural characterisation of UBR5 revealed a large helical scaffold decorated with numerous protein-interacting modules, giving UBR5 a range of possible mechanisms of substrate engagement. We characterise the functional implications of these domains, which collectively suggest multivalent and possibly multimodal substrate recognition mechanisms. Therefore, the potential exists to selectively target UBR5 functions in different substrate and cellular contexts for cancer therapeutics.

An added complexity of investigating UBR5, or dissecting its mechanism, is the homodimeric scaffold, a feature that is not commonly reported for HECT-type E3 ligases. We show that UBR5 dimers further assemble into tetrameric and higher oligomeric states. While many E3s dimerise (Ronchi *et al*, 2014), few are reported to form higher oligomeric states, and the function of these higher-order states is often unclear. We assigned the oligomerisation properties to the previously uncharacterised SBB2 domains and showed that oligomerisation is not imperative for enzymatic function. The elegant assembly of UBR5 protomers into dimers and tetramers may function in positioning each protein-binding module in the vicinity of a catalytic HECT domain rather than directly mediating processivity. The ring-shaped architecture is reminiscent of several monomeric and multimeric E3 enzymes such as HUWE1, GID, BIRC6 or the SCF, where this shape promotes substrate recruitment and ubiquitination (Grabarczyk *et al*, 2021; Hunkeler *et al*, 2021; Sherpa *et al*, 2021; Welcker *et al*, 2022; Dietz *et al*, 2023; Ehrmann *et al*, 2023).

Furthermore, our interpretation of the UBR5 structure agrees well with the findings of the recently published study, which similarly portrays UBR5 as a homodimer that further assembles into a tetramer formation (Wang *et al*, 2023). There is an agreeable consistency between these structures, aside from the extent of the dimerisation interface. Both investigations pinpoint this interface as mediated mainly by a single central helix. Our UBR5 density does not clearly show the "domain-swapped dimerisation loop", and the impact of this region on dimerisation remains to be further investigated. In line with our mutagenesis data, we believe this loop is not integral to the process of dimerisation.

Our experiments further explored the dynamics of HECT E3 ligases. UBR5's large and mobile architecture and the conformational flexibility of the α-solenoid scaffold may position substrates bound to substrate-binding modules in close proximity to multiple HECT domains (Fig 5A and B). This could facilitate ubiquitination

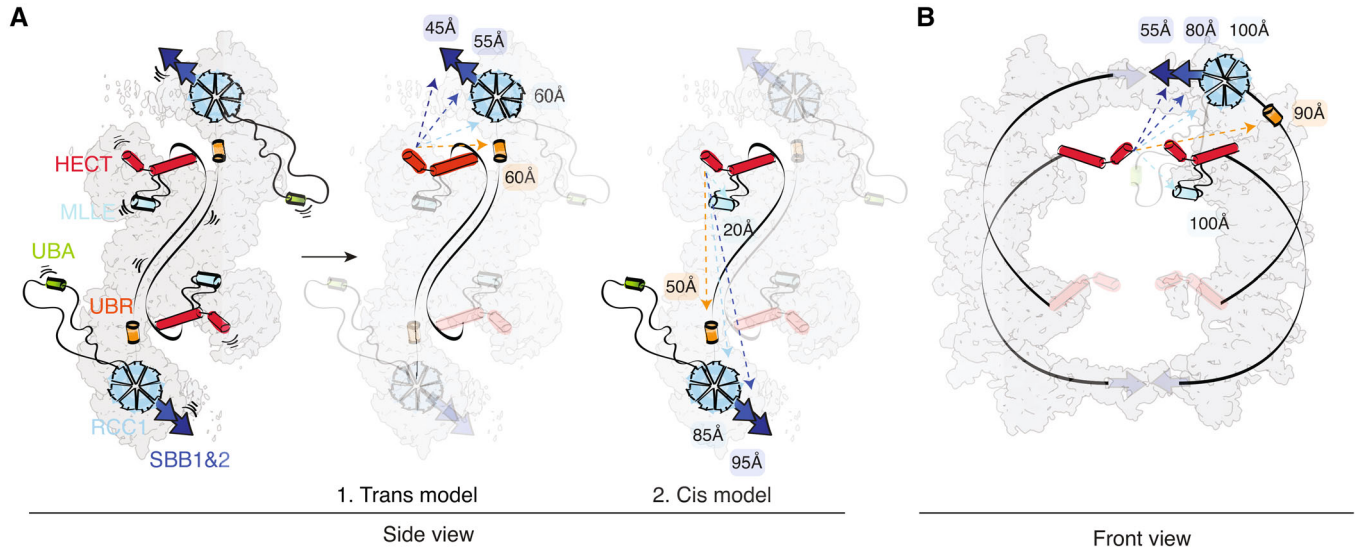

Figure 5. Hypothetical mechanisms for substrate engagement and ubiquitination by UBR5.

A Approximate distances of the protein–protein interacting motifs to the catalytic cysteine of the UBR5 HECT, in *cis* and *trans* of a dimer. Domains are coloured as in Fig 2A.

B Approximate distances between a catalytic domain and protein–protein interacting motifs of two opposite dimers in the tetrameric UBR5 assembly.

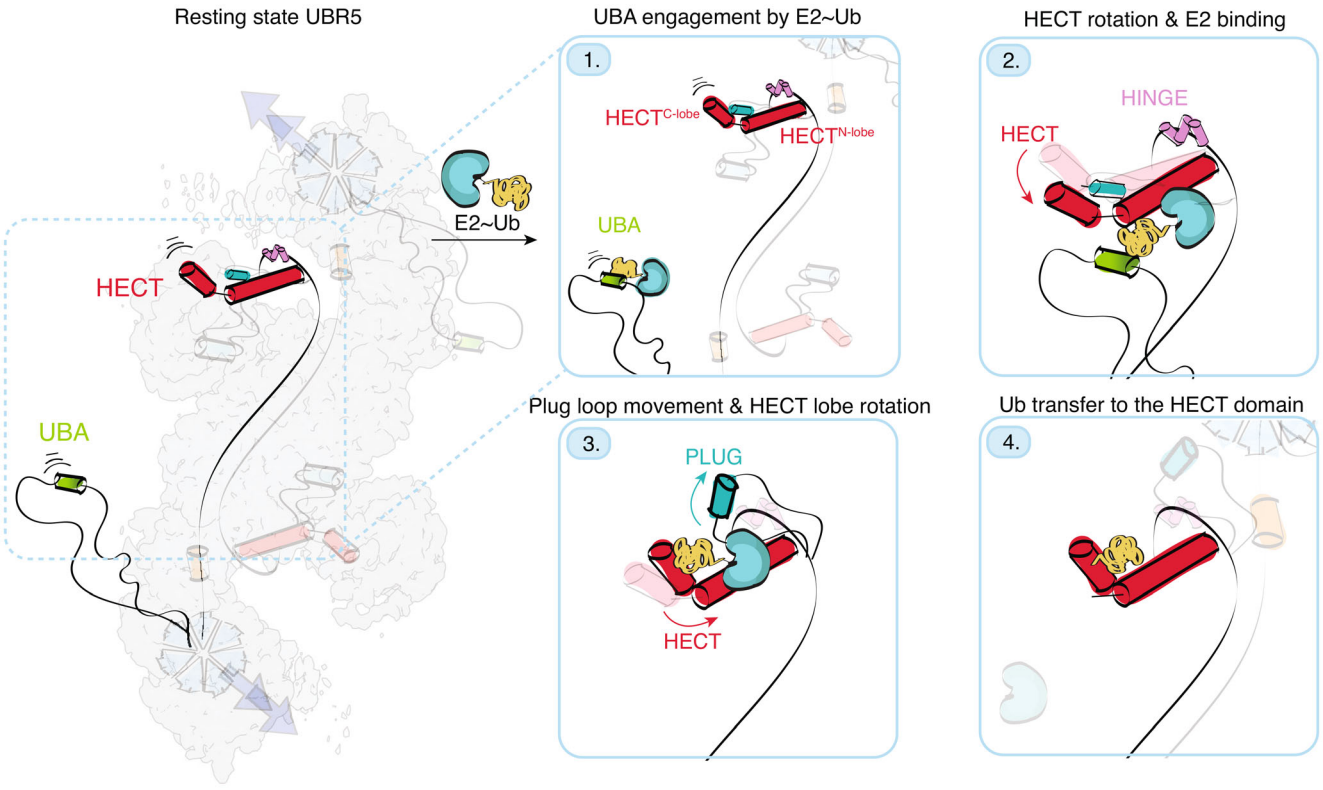

Figure 6. A model of UBR5 domain dynamics for ubiquitin transfer.
Based on our obtained data, we propose the UBA domain mediates the recruitment of Ub-loaded E2 (E2 ~ Ub) to UBR5 (1.). Rotations in the HECT domain, presumably through the flexibility of the hinge region, allow E2 ~ Ub engagement to the HECT domain N-lobe (2.). Transfer of ubiquitin from the E2 to the HECT domain C-lobe is presumably preceded by the removal of the plug loop to allow lobe rotation (3.). Together the movements in the HECT domain lead to UBR5 loading with ubiquitin for substrate ubiquitination (4.).

in *cis* and in *trans*: engaging the substrate through one protomer and mediating ubiquitin transfer with the other, either within a dimer or two opposite dimers of a tetramer. UBR5 flexibility is also visible within the HECT domain itself. We describe two structural features, the plug loop and hinge. The hinge region is also found in the full-length HUWE1 protein (Hunkeler *et al*, 2021), whilst the plug loop appears unique to UBR5. Yet, structural features of other HECT E3 ligases, including Smurf2 or ITCH, contain elements positioned similarly to the plug loop, which govern their activity (Mari *et al*, 2014; Riling *et al*, 2015). Comparing our findings to previous observations, these features could be crucial for ubiquitin transfer and chain assembly (Fig 6).

The function of UBR5 oligomerisation remains an open question. As we observe no loss in ubiquitination activity, these assemblies could instead be important for substrate binding. Whilst smaller or single-chain substrates may benefit from dimeric assemblies, larger complexes could bind through multivalent interactions and require UBR5 to adopt a larger tetrameric state. For example, the mitotic checkpoint complex is composed of several components which bind UBR5 directly (Kaisari *et al*, 2022). In these cases, tetrameric assemblies may modulate such interactions. A recent study has proposed UBR5 to target orphaned proteins which failed to assemble into their destined complexes, particularly at transcriptionally active sites (Oh *et al*, 2020; preprint: Mark *et al*, 2022). The multivalent interactions possible with large UBR5 oligomeric assemblies are not exclusive of this observation, and it remains to be seen which UBR5 oligomeric states can engage orphaned proteins *in vivo*.

Using our recombinant system, we identified AKIRIN2 as a direct interacting partner of UBR5. Using AKIRIN2 as a substrate, we observed that only AKIRIN2 carrying a monoubiquitin modification was efficiently ubiquitinated by UBR5. The chain elongation function of UBR5 is further exhibited when only free ubiquitin was used as the substrate. Therefore, our data suggest that UBR5 is a chain-elongating E3 ligase which first needs to be presented with a monoubiquitinated substrate or recruited together with other chain-initiating enzymes (Yau *et al*, 2017). While our recombinant system may be missing a key post-translational modification or an additional component to directly target the protein substrate, the concept of a handoff or sequential mechanism is a recurring theme, especially when branched ubiquitin chains (ubiquitin simultaneously modified at multiple lysines) are formed (Brown *et al*, 2016; Haakonsen & Rape, 2019).

We further observed an enhanced binding of a pre-ubiquitinated AKIRIN2 to UBR5, and weak binding of pre-ubiquitinated SECURIN, showing that UBR5 could form transient interactions with pre-ubiquitinated substrates necessary for ubiquitin chain elongation. In the case of UbAKIRIN2, the interaction is reminiscent of an avidity engagement mechanism. Whilst the interaction of UBR5 with

AKIRIN2 may also serve a more specialised function, an avidity binding mechanism could be a means of selection preference of certain substrates to achieve their fast turnover and a swift response to cellular stimuli.

Though many questions still remain about the polyubiquitination mechanism of UBR5, the presented structural information expands on our knowledge of the activity of HECT E3 ligases. We initially hypothesised the UBA domain is involved in ubiquitin recognition during ubiquitination and substrate engagement. Whilst the former stands true upon the UBA domain deletion, our ubiquitinated substrate was still able to engage UBR5, suggesting another undefined ubiquitin-binding site exists. HUWE1 possesses numerous ubiquitin-binding modules dispersed across its solenoid ring structure (Grabarczyk *et al*, 2021; Hunkeler *et al*, 2021), which we did not identify in UBR5. Furthermore, the ubiquitin exosite identified in several other HECT E3 ligases appears to be occluded by the MLLE linkers in UBR5 (French *et al*, 2009; Ogunjimi *et al*, 2010; Maspero *et al*, 2011). The existence of such a ubiquitin-binding motif in UBR5 remains to be investigated.

UBR5 presents an intriguing target to therapeutically modulate the fate of a range of its cellular targets. The complex structure and oligomerisation properties of UBR5 presented in this study begin to explain its broad implications in cancer biology (Shearer *et al*, 2015). While UBR5's chain-elongating properties do not strictly control the fate of a given substrate, they can regulate concentrations of its intracellular targets, such as MYC, without being lethal to non-cancerous cells (Qiao *et al*, 2020; de Almeida *et al*, 2021). Our findings on this complex full-length HECT E3 ligase may thus provide a framework for new therapeutics for UBR5-driven diseases.

Materials and Methods

Reagents and Tools table

Reagent/Resource	Reference or Source	Identifier or Catalog Number
Experimental Models		
FreeStyle 293-F	ThermoFisher	R79007
High-Five insect cells	ThermoFisher	B85502
BL21 (DE3)	IMP MolBioService	
DH10EmBacY	IMP MolBioService	
Rosetta2 (DE3)	IMP MolBioService	
Recombinant DNA		
piggyBac – His_{10}-3C-UBR5-TwinStrep	This study	–
pMEPi-TwinStrep-3C-UBR5	This study	
pMEPi-TwinStrep-3C-$UBR5^{mutant}$	This study (Appendix Table S1)	
pFB12-TwinStrep-3C-UBR5	This study	
pET33-His_6-GST-3C-Akirin2	de Almeida et al (2021)	
pET21d-His_6-UBA1	Kamadurai *et al* (2013)	
pET3a-UbWT	Pickart and Raasi (2005)	
pGEX-GST-TEV-Cys-$Ub^{\Delta GG}$	This study	
pET-His_6-eGFP-3C-$Ub^{\Delta GG}$-Akirin2	This study	
pET33-GST-3C-$UBR5^{HECT}$	This study	
Twist-His_6-3C-UBCH5B	This study	
pGEX-GST-TEV-SGGGS-UbSecurin-GGCG-His_6	Yamaguchi *et al* (2015)	
Chemicals, Enzymes and other reagents		
Octyl Maltoside, Fluorinated, Anagrade	Anatrace	O310F
Strep HP column	Cytiva	28907548
Superose™ 6 Increase 10/300 GL	Cytiva	29091596
FreeStyle™ 293 Expression Medium	Thermo Fisher	12338026
SYPRO™ Orange Protein Gel Stain	Thermo Fisher	S6650
CHAPSO	Carl Roth	HN73.2
Software		
Cryosparc 3.1	Punjani *et al* (2017)	
DeepEMhancer	Sanchez-Garcia *et al* (2021)	
AlphaFold2	Jumper *et al* (2021)	
ISOLDE	Croll (2018)	
Coot	Emsley and Cowtan (2004)	
Phenix	Adams *et al* (2010)	
ChimeraX	Goddard *et al* (2017)	
Other		
ÄKTA pure	Cytiva	
Refeyn	Refeyn	
CFX96 Touch Real-Time PCR Detection System	Bio-Rad	
Titan Krios G4	ThermoFisher	
QF R1.2/1.3 on 200 mesh Cu	Quantifoil	X-101-CU200

Methods and Protocols

Constructs and HEK cell lines

The codon-optimised sequence of full-length human UBR5 was purchased from Twist Bioscience as DNA fragments and cloned into pMEPI plasmid as two constructs (UBR5 and $UBR5^{wt}$). For single-particle analysis, the UBR5 construct included a decahistidine (10×His) tag followed by a Prescission protease (3C) cleavage site,

the codon-optimised UBR5 sequence and a double strep tag. For all activity assays, the UBR5^{wt} construct and its derivates included a double strep tag followed by a 3C site and the codon-optimised UBR5 sequence. Mutations and deletions introduced to UBR5^{wt} are listed in Appendix Table S1. The constructs were used for the generation of stable HEK293T cell lines, generated by co-transfecting the constructs under the control of a Tet inducible promoter bearing a puromycin selection marker and the PiggyBac transposase for stable genomic integration. Cells were cultured in FreeStyle 293 Expression Medium (GIBCO). Protein expression was induced by the addition of doxycycline at a final concentration of 1 μg/ml for 48 h. Twenty-four hours post-induction, 125 ml of Ex-Cell 293 Serum-Free Medium (Sigma Aldrich) was added per 0.5 l of culture. Cells were harvested by centrifugation at 2,000 *g* for 20 min. Pellets were washed in 1×PBS and flash-frozen in liquid nitrogen for storage at −70°C.

Constructs for E. coli expression

The codon-optimised sequence of the human UBR5 HECT domain (residues 2,217–2,312, GS linker, and 2,501–2,799) was purchased from Twist Bioscience as DNA fragments and cloned into a pET33 vector for *E. coli* expression containing a hexahistidine (6×His) tag followed by a Glutathione-S-transferase (GST) tag and a 3C site. For ^{GFP}AKIRIN2, the human AKIRIN2 sequence was cloned into a pGEX vector containing an N-terminal 6×His tag, followed by GFP and a 3C cleavage site. For ^{GFP}UbAKIRIN2, the sequence coding for ubiquitin without the last two C-terminal amino acids (sequence "GG") was inserted immediately before the AKIRIN2-coding sequence. UBCH5B was purchased as a clone in a Twist-6xHis-3C plasmid (Twist Bioscience). For protein expression of UBR5^{HECT} and AKIRIN2-containing constructs, BL21 (DE3) cells were chemically transformed as per standard protocol. UBCH5B was expressed in Rosetta2 (DE3) competent cells. All three constructs were grown in autoinduction media at 37°C, and expression was induced overnight at 18°C. Cells were harvested by centrifugation at 2000x*g* for 20 min.

Ubiquitin with a deletion of the two C-terminal residues, GG (Ub$^{\Delta GG}$), was cloned into a pGEX–TEV vector, preceded by a single cysteine for labelling, a TEV cleavage site and a GST tag (GST-TEV-Cys-Ub$^{\Delta GG}$). For protein expression, BL21 (DE3) RIL-competent cells were chemically transformed as per standard protocol. Cells were grown in Luria Broth (LB) medium at 37°C until cells reached OD_{600} 0.8–1.0. Expression was induced with 0.6 mM IPTG, and the temperature was reduced to 23°C overnight.

Constructs for insect cell expression

All constructs for expression in insect cells were cloned into the pFB12 vector under the polyhedrin promoter, carrying an N-terminal double strep tag, followed by a 3C site. The plasmids were transformed into DH10EmBacY chemically competent cells. Positive clones were selected using the blue/white screening. The bacmid was purified using the isopropanol precipitation method and recombination of the gene of interest was verified by PCR. The bacmid was transfected into Sf9 cells using polyethyleneimine (PEI) for the generation of the V0 stock, using YFP fluorescence as a measure of transfection efficiency. Following virus amplification in Sf9 suspension insect cell culture, constructs were expressed in *Trichoplusia ni* High-Five insect cells (Thermo Fisher) infected at a density of 1×10^{-6}/ml using the appropriate virus. Cells were grown at 27°C at 100 rpm shaking using ESF921 serum-free growth medium (Expression Systems). Cells were harvested 3 days after transfection by centrifugation at 2,000 *g* for 20 min, and pellets were flash-frozen in liquid nitrogen and stored at −80°C.

Protein purification

For all full-length UBR5 constructs, the cell pellet was resuspended in 3× (w/v) of BufferA (50 mM HEPES/NaOH pH 8.0, 300 mM NaCl, 0.5 mM TCEP) supplemented with complete protease inhibitor cocktail tablets (Roche) and Benzonase (IMP Molecular Biology Service) Cells were lysed using a glass Dounce homogeniser and subsequently centrifuged for 1 h at 40,000 *g*. The supernatant was applied on a pre-equilibrated StrepTrap HP column (Cytiva) equilibrated in buffer A. The column was washed with 10 column volumes (CV) of BufferA and eluted with BufferA supplemented with 5 mM desthiobiotin. The eluate was collected as fractions and combined, concentrated with a 100 kDa cut-off concentrator (Cytiva), and loaded on a Superose 6 10/300 column (Cytiva) equilibrated in GF Buffer (50 mM HEPES/NaOH pH 7.5, 150 mM NaCl, 1 mM TCEP). For long-term storage, the desired fractions were combined, concentrated and flash-frozen in liquid nitrogen. For cryo-EM sample preparation, the sample was taken from a single fraction of the SEC elution peak and plunge-frozen directly.

For UBR5^{HECT}, the cell pellet was resuspended in 3× (w/v) of BufferA (50 mM HEPES/NaOH pH 8.0, 500 mM NaCl, 0.5 mM TCEP) supplemented with complete protease inhibitor cocktail tablets and Benzonase (IMP Molecular Biology Service) Cells were lysed using a cell disruptor (Constant systems Ltd) at a pressure set to 1.4 kPa and subsequently centrifuged for 1 h at 40,000 *g*. The supernatant was applied on a pre-equilibrated GST Trap HP column (Cytiva) equilibrated in buffer A. The column was washed with 10 column volumes (CV) of BufferA and eluted with BufferA supplemented with 15 mM glutathione. The eluate was collected as fractions and combined and loaded on a Superdex 200 16/60 column (Cytiva) equilibrated in GF Buffer (50 mM HEPES/NaOH pH 7.5, 150 mM NaCl, 0.5 mM TCEP). For long-term storage, the desired fractions were combined, concentrated and flash-frozen in liquid nitrogen.

For ^{GFP}AKIRIN2 and ^{GFP}UbAKIRIN2, the cell pellet was resuspended in Buffer H (50 mMTris-HCll pH 8, 500 mM NaCl, 0.5 mM TCEP) supplemented with complete protease inhibitor cocktail and Benzonase. The cell suspension was homogenised using French Press at 1.5 kBar and subsequently centrifuged for 1 h at 40,000 *g*. The supernatant was applied on a 5 ml HisTrap HP column (Cytiva) pre-equilibrated with buffer H. Column was washed with 10CV of 5% of buffer E (50 mM TrisHcl pH 8, 500 mM NaCl, 0.5 mM TCEP, 500 mM Imidazole pH 8) and eluted with 50% of buffer E. Fractions were pooled, concentrated with a 30 kDa cut-off concentrator (Cytiva) and loaded on a Superdex S200 16/60 column (Cytiva) equilibrated in GF Buffer. Desired fractions were pooled, concentrated and flash-frozen in liquid nitrogen for long-term storage.

For UBCH5B, cells were resuspended in BufferU-A (20 mM Tris pH 8.0, 500 mM NaCl, 0.5 mM TCEP) supplemented with complete protease inhibitor cocktail and Benzonase. The cell suspension was homogenised using French Press at 1.5 kBar and subsequently centrifuged for 1 h at 40,000 *g*. The supernatant was applied on a 5 ml HisTrap HP column (Cytiva) pre-equilibrated with BufferU-A,

and protein eluted using a gradient of Buffer U-A and BufferU-B (BufferA supplemented with 500 mM Imidazole pH 8). The tag was cleaved overnight using Precission protease and subsequently passed through a HisTrap HP column to capture the cleaved tag and protease. Protein was concentrated and loaded onto a Superdex 75 16/60 column (Cytiva) pre-equilibrated with BufferU-GF (20 mM HEPES pH 8.0, 50 mM NaCl, 1 mM DTT). Desired fractions were pooled, concentrated and flash-frozen in liquid nitrogen for long-term storage.

For wild-type ubiquitin (wtUbiquitin), cells were resuspended in BufferUbi (50 mM Tris 7.5, 300 mM NaCl) supplemented with complete protease inhibitor cocktail and Benzonase. The cell suspension was homogenised using French Press at 1.5 kBar and subsequently centrifuged for 1 h at 40,000 *g*. Glacial acetic acid was slowly added to the supernatant until reaching pH 4.5, followed by centrifugation at 15,000 *g* for 30 min. The supernatant was then dialysed overnight into 25 mM sodium acetate (NaAc) pH 4.5. The dialysed sample was concentrated and loaded on a pre-equilibrated Resource S column (Cytiva) in 25 mM NaAc pH 4.5. Protein was eluted with a shallow gradient of 25 mM NaAc, pH 4.5, and 25 mM NaAc, pH4.5, and 250 mM NaCl. Desired fractions were concentrated using a 5 kDa cut-off concentrator (Cytiva) and loaded on a Superdex 75 16/60 column (Cytiva) pre-equilibrated with buffer composed of 25 mM HEPES pH 8 and 50 mM NaCl.

For $Ub^{\Delta GG}$, cells were pelleted at 3,000 *g*, resuspended in BufferT (50 mM Tris pH 7.6, 200 mM NaCl), and lysed by sonication. The lysate was cleared by centrifugation at 15,000 *g* and incubated with anti-GS4B resin for 2 h at 4°C (Genessee Scientific). The resin was washed with excess BufferT and TEV protease was added to beads rocking overnight at RT. The resin was pelleted at 500 *g*, the supernatant containing $Ub^{\Delta GG}$ was removed and stored, and resin was resuspended in a small amount of BufferT. Excess $Ub^{\Delta GG}$ was washed off of resin with more Buffer T. Supernatant and wash were combined, centrifuged at 4,000 *g* to remove precipitated protein, concentrated, and purified using Ni–NTA Superflow beads (Qiagen) and GS4B resins to final purity. Protein was concentrated and flash-frozen in liquid nitrogen for long-term storage.

Labelling of $Ub^{\Delta GG}$ was performed as described previously (Brown *et al*, 2014). Briefly, the protein was reduced by adding 20 mM DTT and desalted twice into 50 mM HEPES pH 7.0, 200 mM NaCl. Cy5-maleimide was resuspended in DMSO and added in 2.5 molar excess to the protein, followed by 2 h incubation at RT. Cy5-$Ub^{\Delta GG}$ was dialysed overnight against 50 mM HEPES pH 8.0, 200 mM NaCl, followed by desalting to remove excess dye. The labelled protein was stored at −80°C.

Securin purification and fluorescent labelling was performed as described previously (Welsh *et al*, 2022). Recombinant human UBA1 was provided by the Vienna BioCenter core facilities and purified as described elsewhere (Grabarczyk *et al*, 2021).

Ubiquitination assays

All reactions were prepared by mixing reaction components in assay buffer (100 mM NaCl, 20 mM HEPES pH 8, 5 mM $MgCl_2$) on ice. Reactions were performed at the indicated temperatures (25 or 37°C) with the following final concentrations: HisUBA1 at 0.3 μM, UBCH5b at 2.5 μM, $UBR5^{wt}$ at 0.2 μM or 0.3 μM (as indicated in figure captions), wtUbiquitin at 20 μM, the substrate at 2 μM. Reactions were initiated by the addition of 2 mM ATP and collected at the indicated time points. Timepoint zero was taken prior to addition of ATP. Substrate ubiquitination was visualised using fluorescence imaging using a ChemiDoc MP System (BioRad). Protein content was visualised using stain-free imaging. Gels were subsequently stained with Coomassie blue to visualise ubiquitin content.

E2 screen (E2 Scan Kit version 2, Ubiquigent) was performed guided by the manufacturer's instructions. Briefly, concentrations of components of the reactions were used as described above, except that a mixture of wtUbiquitin and ^{FAM}ubiquitin was used to visualise autoubiquitination. Incubation was performed at 37°C for 30 min. Results were visualised using a ChemiDocMP System (BioRad) using fluorescence imaging and stain-free imaging.

Sucrose gradient preparation

Density gradient centrifugations were performed by preparing the low-density solution of 10% (w/v) sucrose and high-density solution of 30% (w/v) sucrose in GF buffer. Gradients were made by mixing the two solutions using the Gradient Master (Biocomp systems) to create a continuous sucrose gradient. All compared gradients were performed in parallel using the same input protein concentrations (40 pmol for each input protein). The sample was applied onto the density gradient prepared in an open-top 4.2 ml ultracentrifuge tube and run for 16 h at 105,350 *g* in an SW60Ti rotor. Gradients were manually fractionated into 200 μl fractions and analysed with stain-free and fluorescence imaging using ChemiDocMP System (BioRad) for UBR5 and FAM/GFP-labelled substrates, respectively.

Protein sequence analysis

Sequences of 39 metazoan UBR5 species were collected from the UniProt reference database (UniProt Consortium, 2021) in a NCBI-Blast search applying highly significant E-value thresholds (< 1e-50; Altschul *et al*, 1997) and aligned with MAFFT (v7.505, –linsi method; Katoh & Toh, 2008). Visualisation was performed with Jalview (Waterhouse *et al*, 2009). Six species were selected as a representative pool, shown in Appendix Fig S3.

Cryo-EM sample preparation and data collection

All constructs analysed by cryo-EM were prepared in the following way: Open-hole R1.2/1.3 grids (Quantifoil) with 200 mesh were used for plunge freezing. Grids were glow-discharged with BalTec SCD 005 sputter coater for 120 s at 25 mA using residual air. Four microliters of the sample was applied onto the treated side and front-side blotted using the Leica GP2 plunge freezer. UBR5 constructs were frozen in GF Buffer with the addition of 4 mM CHAPSO or 0.005% (w/v) fluorinated octyl β-maltoside (Anatrace) prior to freezing.

Initial grid screening was performed on the 200 kV Glacios microscope (ThermoFisher) using the Falcon III detector (ThermoFisher). For high-resolution structure determination, data collection was performed on a 300 kV Titan Krios G4 equipped with a cold field emission gun and a post-column Selectris energy filter (ThermoFisher) with a 5 eV slit width and a Falcon 4 or Falcon 4i direct electron detector (ThermoFisher). Images were collected at a pixel size of 0.745 Å/pix or 0.951 Å/pix with a cumulative dose of $40e^-/Å^2$ for untilted, and 50e−/Å2 for 30° tilted images, in eer format, using a defocus range in 0.3 μm increments (Appendix Fig S2).

Cryo-EM image processing and model refinement

On-the-fly preprocessing (patch motion correction and CTF estimation) was performed using Cryosparc Live. All steps are described in Appendix Fig S2. Briefly, particles were first manually picked in Cryosparc 3.1 (Punjani *et al*, 2017) to generate templates for template picking, which was performed on manually curated micrographs. Following template-based picking, particles were classified using reference-free 2D classification, followed by ab-initio reconstruction and heterogeneous refinement. The best resulting 3D volume was subjected to several rounds of homogeneous and local refinements using half-map masks generated in ChimeraX. Final models were sharpened using the DeepEMhancer tool (Sanchez-Garcia *et al*, 2021). Merged maps from local refinements used to generate model 2 for model building were generated using ChimeraX. The initial model for model building was generated using the AlphaFold2 prediction software (Jumper *et al*, 2021). The predicted model was docked twice onto the maps and manually edited using Coot and ISOLDE (Croll, 2018). Real-space refinement was performed using Phenix (Afonine *et al*, 2018). Map 1 was used for initial model building. After the collection and reconstruction of Map 2, this model was used for final model building.

Mass photometry

Measurements were performed as described in (Sonn-Segev *et al*, 2020). Briefly, OneMP (Refeyn) was calibrated using the Native protein marker as a protein standard using a medium field of view. MP signals were collected for 60 s to detect at least 5,000 individual molecules. Each measurement was performed at a final protein concentration of 100 nM. Raw data were processed using the DiscoverMP software and plotted as histograms of molar mass distributions.

ThermoFluor

Melting temperatures of UBR5 constructs were determined using ThermoFluor (Cummings *et al*, 2006). Briefly, samples were diluted in SEC buffer to a final concentration of 0.3 mg/ml in 20 µl. One microliter of 20× SyproOrange dye was used per measurement. The fluorescence of SyproOrange dye upon protein unfolding was measured using an RT–PCR machine (CFX-Touch, BioRad). A temperature gradient ranging from 15 to 95°C was applied, using 0.5°C increments.

Mass spectrometry

LC–MS/MS analysis was performed on a nano HPLC system (UltiMate 3000 RSLC nano system, Thermo Fisher Scientific) coupled to an Orbitrap Exploris 480 mass spectrometer equipped with a FAIMS pro interfaces and a Nanospray Flex ion source. The peptides were loaded onto a trap column (PepMap Acclaim C18, 5 mm × 300 µm ID, 5 µm particles, 100 Å pore size, Thermo Fisher Scientific) at a flow rate of 25 µl/min using 0.1% TFA as mobile phase. After 10 min, the trap column was switched in line with the analytical column (PepMap Acclaim C18, 500 mm × 75 µm ID, 2 µm, 100 Å, Thermo Fisher Scientific) operated at 30°C. Peptides were eluted using a flow rate of 230 nl/min, starting with the mobile phases 98% A (0.1% formic acid in water) and 2% B (80% acetonitrile, 0.1% formic acid) and linearly increasing to 35% B over the next 60 min. Mass spectra were collected in positive ionisation mode using data-dependent acquisition and product ions generated using HCD.

Data availability

Atomic coordinates and cryo-EM density maps have been deposited in the Protein Data Bank (PDBe) under accession codes PDB:8BJA (https://www.rcsb.org/structure/8BJA), and EMD-16087 (https://www.ebi.ac.uk/emdb/EMD-16087). The raw micrographs were submitted to the EMPIAR database under accession code EMPIAR-11501 (https://www.ebi.ac.uk/empiar/EMPIAR-11501). Other source data are included as attachments to the manuscript.

Expanded View for this article is available online.

Acknowledgements

We thank all members of the Haselbach and Brown lab for discussions on the project, the Electron Microscopy, ProTech and Mass Spectrometry facilities from the Vienna Biocenter Core Facilities for their support. ZH received funding from the European Union's Framework Programme for Research and Innovation Horizon 2020 (2014-2020) under the Marie Curie Skłodowska Grant Agreement Nr. 847548. HLB was generously supported by Boehringer Ingelheim (BI1982). IMP was supported by Boehringer Ingelheim. The Brown lab was supported by NIH T32GM008570 (DLB) and NIH R35GM128855 (NGB).

Author contributions

Zuzana Hodáková: Conceptualization; data curation; formal analysis; funding acquisition; validation; investigation; visualization; methodology; writing – original draft; writing – review and editing. **Irina Grishkovskaya:** Data curation; investigation; methodology. **Hanna L Brunner:** Investigation; writing – review and editing. **Derek L Bolhuis:** Investigation; writing – review and editing. **Katarina Belačić:** Investigation. **Alexander Schleiffer:** Data curation; methodology. **Harald Kotisch:** Methodology. **Nicholas G Brown:** Conceptualization; resources; data curation; supervision; funding acquisition; validation; methodology; writing – original draft; writing – review and editing. **David Haselbach:** Conceptualization; resources; data curation; supervision; funding acquisition; validation; writing – original draft; project administration; writing – review and editing.

Disclosure and competing interests statement

The authors declare that they have no conflict of interest.

References

Adams PD, Afonine PV, Bunkóczi G, Chen VB, Davis IW, Echols N, Headd JJ, Hung L-W, Kapral GJ, Grosse-Kunstleve RW *et al* (2010) PHENIX: a comprehensive Python-based system for macromolecular structure solution. *Acta Crystallogr D Biol Crystallogr* 66: 213 – 221

Afonine PV, Poon BK, Read RJ, Sobolev OV, Terwilliger TC, Urzhumtsev A, Adams PD (2018) Real-space refinement in PHENIX for cryo-EM and crystallography. *Acta Crystallogr D Struct Biol* 74: 531 – 544

de Almeida M, Hinterndorfer M, Brunner H, Grishkovskaya I, Singh K, Schleiffer A, Jude J, Deswal S, Kalis R, Vunjak M *et al* (2021) AKIRIN2 controls the nuclear import of proteasomes in vertebrates. *Nature* 599: 491 – 496

Altschul SF, Madden TL, Schäffer AA, Zhang J, Zhang Z, Miller W, Lipman DJ (1997) Gapped BLAST and PSI-BLAST: a new generation of protein database search programs. *Nucleic Acids Res* 25: 3389 – 3402

Brown NG, Watson ER, Weissmann F, Jarvis MA, VanderLinden R, Grace CRR, Frye JJ, Qiao R, Dube P, Petzold G *et al* (2014) Mechanism of

polyubiquitination by human anaphase-promoting complex: RING repurposing for ubiquitin chain assembly. *Mol Cell* 56: 246 – 260

Brown NG, VanderLinden R, Watson ER, Weissmann F, Ordureau A, Wu K-P, Zhang W, Yu S, Mercredi PY, Harrison JS *et al* (2016) Dual RING E3 architectures regulate multiubiquitination and ubiquitin chain elongation by APC/C. *Cell* 165: 1440 – 1453

Cammarata-Mouchtouris A, Nguyen X-H, Acker A, Bonnay F, Goto A, Orian A, Fauvarque M-O, Boutros M, Reichhart J-M, Matt N (2020) Hyd ubiquitinates the NF-κB co-factor Akirin to operate an effective immune response in drosophila. *PLoS Pathog* 16: e1008458

Chari A, Haselbach D, Kirves J-M, Ohmer J, Paknia E, Fischer N, Ganichkin O, Möller V, Frye JJ, Petzold G *et al* (2015) ProteoPlex: stability optimization of macromolecular complexes by sparse-matrix screening of chemical space. *Nat Methods* 12: 859 – 865

Choi WS, Jeong B-C, Joo YJ, Lee M-R, Kim J, Eck MJ, Song HK (2010) Structural basis for the recognition of N-end rule substrates by the UBR box of ubiquitin ligases. *Nat Struct Mol Biol* 17: 1175 – 1181

Cipolla L, Bertoletti F, Maffia A, Liang C-C, Lehmann AR, Cohn MA, Sabbioneda S (2019) UBR5 interacts with the replication fork and protects DNA replication from DNA polymerase η toxicity. *Nucleic Acids Res* 47: 11268 – 11283

Clancy JL, Henderson MJ, Russell AJ, Anderson DW, Bova RJ, Campbell IG, Choong DYH, Macdonald GA, Mann GJ, Nolan T *et al* (2003) EDD, the human orthologue of the hyperplastic discs tumour suppressor gene, is amplified and overexpressed in cancer. *Oncogene* 22: 5070 – 5081

Croll TI (2018) ISOLDE: a physically realistic environment for model building into low-resolution electron-density maps. *Acta Crystallogr D Struct Biol* 74: 519 – 530

Cummings MD, Farnum MA, Nelen MI (2006) Universal screening methods and applications of ThermoFluor. *J Biomol Screen* 11: 854 – 863

Deo RC, Sonenberg N, Burley SK (2001) X-ray structure of the human hyperplastic discs protein: an ortholog of the C-terminal domain of poly (a)-binding protein. *Proc Natl Acad Sci U S A* 98: 4414 – 4419

Dietz L, Ellison CJ, Riechmann C, Cassidy CK, Felfoldi FD, Pinto-Fernández A, Kessler BM, Elliott PR (2023) Structural basis for SMAC-mediated antagonism of caspase inhibition by the giant ubiquitin ligase BIRC6. *Science* 379: 1112 – 1117

Ehrmann JF, Grabarczyk DB, Heinke M, Deszcz L, Kurzbauer R, Hudecz O, Shulkina A, Gogova R, Meinhart A, Versteeg GA *et al* (2023) Structural basis for regulation of apoptosis and autophagy by the BIRC6/SMAC complex. *Science* 379: 1117 – 1123

Emsley P, Cowtan K (2004) Coot: model-building tools for molecular graphics. *Acta Crystallogr D Biol Crystallogr* 60: 2126 – 2132

Flack JE, Mieszczanek J, Novcic N, Bienz M (2017) Wnt-dependent inactivation of the Groucho/TLE Co-repressor by the HECT E3 ubiquitin ligase Hyd/UBR5. *Mol Cell* 67: 181 – 193

French ME, Kretzmann BR, Hicke L (2009) Regulation of the RSP5 ubiquitin ligase by an intrinsic ubiquitin-binding site. *J Biol Chem* 284: 12071 – 12079

García-Cano J, Martinez-Martinez A, Sala-Gaston J, Pedrazza L, Rosa JL (2019) HERCing: structural and functional relevance of the large HERC ubiquitin ligases. *Front Physiol* 10: 1014

Goddard TD, Huang CC, Meng EC, Pettersen EF, Couch GS, Morris JH, Ferrin TE (2017) UCSF ChimeraX: meeting modern challenges in visualization and analysis. *Protein Sci* 27: 14 – 25

Grabarczyk DB, Petrova OA, Deszcz L, Kurzbauer R, Murphy P, Ahel J, Vogel A, Gogova R, Faas V, Kordic D *et al* (2021) HUWE1 employs a giant substrate-binding ring to feed and regulate its HECT E3 domain. *Nat Chem Biol* 17: 1084 – 1092

Gudjonsson T, Altmeyer M, Savic V, Toledo L, Dinant C, Grøfte M, Bartkova J, Poulsen M, Oka Y, Bekker-Jensen S *et al* (2012) TRIP12 and UBR5 suppress spreading of chromatin ubiquitylation at damaged chromosomes. *Cell* 150: 697 – 709

Haakonsen DL, Rape M (2019) Branching out: improved signaling by heterotypic ubiquitin chains. *Trends Cell Biol* 29: 704 – 716

Harper JW, Schulman BA (2021) Cullin-RING ubiquitin ligase regulatory circuits: a quarter century beyond the F-box hypothesis. *Annu Rev Biochem* 90: 403 – 429

Henderson MJ, Munoz MA, Saunders DN, Clancy JL, Russell AJ, Williams B, Pappin D, Khanna KK, Jackson SP, Sutherland RL *et al* (2006) EDD mediates DNA damage-induced activation of CHK2. *J Biol Chem* 281: 39990 – 40000

Huang L, Kinnucan E, Wang G, Beaudenon S, Howley PM, Huibregtse JM, Pavletich NP (1999) Structure of an E6AP-UbcH7 complex: insights into ubiquitination by the E2-E3 enzyme cascade. *Science* 286: 1321 – 1326

Hunkeler M, Jin CY, Ma MW, Monda JK, Overwijn D, Bennett EJ, Fischer ES (2021) Solenoid architecture of HUWE1 contributes to ligase activity and substrate recognition. *Mol Cell* 81: 3468 – 3480

Jumper J, Evans R, Pritzel A, Green T, Figurnov M, Ronneberger O, Tunyasuvunakool K, Bates R, Žídek A, Potapenko A *et al* (2021) Highly accurate protein structure prediction with AlphaFold. *Nature* 596: 583 – 589

Kaisari S, Miniowitz-Shemtov S, Sitry-Shevah D, Shomer P, Kozlov G, Gehring K, Hershko A (2022) Role of ubiquitin-protein ligase UBR5 in the disassembly of mitotic checkpoint complexes. *Proc Natl Acad Sci U S A* 119: e2121478119

Kamadurai HB, Souphron J, Scott DC, Duda DM, Miller DJ, Stringer D, Piper RC, Schulman BA (2009) Insights into ubiquitin transfer cascades from a structure of a UbcH5B approximately ubiquitin-HECT(NEDD4L) complex. *Mol Cell* 36: 1095 – 1102

Kamadurai HB, Qiu Y, Deng A, Harrison JS, MacDonald C, Actis M, Rodrigues P, Miller DJ, Souphron J, Lewis SM *et al* (2013) Mechanism of ubiquitin ligation and lysine prioritization by a HECT E3. *Elife* 2: e00828

Kambach C, Walke S, Young R, Avis JM, de la Fortelle E, Raker VA, Lührmann R, Li J, Nagai K (1999) Crystal structures of two Sm protein complexes and their implications for the assembly of the spliceosomal snRNPs. *Cell* 96: 375 – 387

Katoh K, Toh H (2008) Recent developments in the MAFFT multiple sequence alignment program. *Brief Bioinform* 9: 286 – 298

Kim HC, Huibregtse JM (2009) Polyubiquitination by HECT E3s and the determinants of chain type specificity. *Mol Cell Biol* 29: 3307 – 3318

Kim JG, Shin H-C, Seo T, Nawale L, Han G, Kim BY, Kim SJ, Cha-Molstad H (2021) Signaling pathways regulated by UBR box-containing E3 ligases. *Int J Mol Sci* 22: 8323

Komander D, Rape M (2012) The ubiquitin code. *Annu Rev Biochem* 81: 203 – 229

Kozlov G, Nguyen L, Lin T, De Crescenzo G, Park M, Gehring K (2007) Structural basis of ubiquitin recognition by the ubiquitin-associated (UBA) domain of the ubiquitin ligase EDD. *J Biol Chem* 282: 35787 – 35795

Li J, Zhang W, Gao J, Du M, Li H, Li M, Cong H, Fang Y, Liang Y, Zhao D *et al* (2021) E3 Ubiquitin ligase UBR5 promotes the metastasis of pancreatic cancer via destabilizing F-Actin capping protein CAPZA1. *Front Oncol* 11: 634167

Liao L, Song M, Li X, Tang L, Zhang T, Zhang L, Pan Y, Chouchane L, Ma X (2017) E3 ubiquitin ligase UBR5 drives the growth and metastasis of triple-negative breast cancer. *Cancer Res* 77: 2090 – 2101

Ling S, Lin W-C (2011) EDD inhibits ATM-mediated phosphorylation of p53. *J Biol Chem* 286: 14972 – 14982

Lorenz S (2018) Structural mechanisms of HECT-type ubiquitin ligases. *Biol Chem* 399: 127 – 145

Mansfield E, Hersperger E, Biggs J, Shearn A (1994) Genetic and molecular analysis of hyperplastic discs, a gene whose product is required for regulation of cell proliferation in *Drosophila melanogaster* imaginal discs and germ cells. *Dev Biol* 165: 507 – 526

Mari S, Ruetalo N, Maspero E, Stoffregen MC, Pasqualato S, Polo S, Wiesner S (2014) Structural and functional framework for the autoinhibition of Nedd4-family ubiquitin ligases. *Structure* 22: 1639 – 1649

Mark KG, Kolla S, Garshott DM, Martínez-González B, Xu C, Akopian D, Haakonsen DL, See SK, Rapé M (2022) Orphan quality control shapes network dynamics and gene expression. *bioRxiv* https://doi.org/10.1101/2022.11.06.515368 [PREPRINT]

Maspero E, Mari S, Valentini E, Musacchio A, Fish A, Pasqualato S, Polo S (2011) Structure of the HECT:ubiquitin complex and its role in ubiquitin chain elongation. *EMBO Rep* 12: 342 – 349

Maspero E, Valentini E, Mari S, Cecatiello V, Soffientini P, Pasqualato S, Polo S (2013) Structure of a ubiquitin-loaded HECT ligase reveals the molecular basis for catalytic priming. *Nat Struct Mol Biol* 20: 696 – 701

Matta-Camacho E, Kozlov G, Li FF, Gehring K (2010) Structural basis of substrate recognition and specificity in the N-end rule pathway. *Nat Struct Mol Biol* 17: 1182 – 1187

Matta-Camacho E, Kozlov G, Menade M, Gehring K (2012) Structure of the HECT C-lobe of the UBR5 E3 ubiquitin ligase. *Acta Crystallogr Sect F Struct Biol Cryst Commun* 68: 1158 – 1163

Meissner B, Kridel R, Lim RS, Rogic S, Tse K, Scott DW, Moore R, Mungall AJ, Marra MA, Connors JM *et al* (2013) The E3 ubiquitin ligase UBR5 is recurrently mutated in mantle cell lymphoma. *Blood* 121: 3161 – 3164

Muñoz-Escobar J, Matta-Camacho E, Kozlov G, Gehring K (2015) The MLLE domain of the ubiquitin ligase UBR5 binds to its catalytic domain to regulate substrate binding. *J Biol Chem* 290: 22841 – 22850

Muñoz-Escobar J, Matta-Camacho E, Cho C, Kozlov G, Gehring K (2017) Bound waters mediate binding of diverse substrates to a ubiquitin ligase. *Structure* 25: 719 – 729

Ogunjimi AA, Wiesner S, Briant DJ, Varelas X, Sicheri F, Forman-Kay J, Wrana JL (2010) The ubiquitin binding region of the Smurf HECT domain facilitates polyubiquitylation and binding of ubiquitylated substrates. *J Biol Chem* 285: 6308 – 6315

Oh E, Mark KG, Mocciaro A, Watson ER, Prabu JR, Cha DD, Kampmann M, Gamarra N, Zhou CY, Rape M (2020) Gene expression and cell identity controlled by anaphase-promoting complex. *Nature* 579: 136 – 140

Pickart CM, Raasi S (2005) Controlled synthesis of polyubiquitin chains. *Methods Enzymol* 399: 21 – 36

Punjani A, Fleet DJ (2021) 3D variability analysis: resolving continuous flexibility and discrete heterogeneity from single particle cryo-EM. *J Struct Biol* 213: 107702

Punjani A, Rubinstein JL, Fleet DJ, Brubaker MA (2017) cryoSPARC: algorithms for rapid unsupervised cryo-EM structure determination. *Nat Methods* 14: 290 – 296

Qiao X, Liu Y, Prada ML, Mohan AK, Gupta A, Jaiswal A, Sharma M, Merisaari J, Haikala HM, Talvinen K *et al* (2020) UBR5 is coamplified with MYC in breast tumors and encodes an ubiquitin ligase that limits MYC-dependent apoptosis. *Cancer Res* 80: 1414 – 1427

Renault L, Kuhlmann J, Henkel A, Wittinghofer A (2001) Structural basis for guanine nucleotide exchange on ran by the regulator of chromosome condensation (RCC1). *Cell* 105: 245 – 255

Riling C, Kamadurai H, Kumar S, O'Leary CE, Wu K-P, Manion EE, Ying M, Schulman BA, Oliver PM (2015) Itch WW domains inhibit its E3 ubiquitin ligase activity by blocking E2-E3 ligase trans-thiolation. *J Biol Chem* 290: 23875 – 23887

Ronchi VP, Klein JM, Edwards DJ, Haas AL (2014) The active form of E6-associated protein (E6AP)/UBE3A ubiquitin ligase is an oligomer. *J Biol Chem* 289: 1033 – 1048

Sanchez-Garcia R, Gomez-Blanco J, Cuervo A, Carazo JM, Sorzano COS, Vargas J (2021) DeepEMhancer: a deep learning solution for cryo-EM volume post-processing. *Commun Biol* 4: 1 – 8

Sander B, Xu W, Eilers M, Popov N, Lorenz S (2017) A conformational switch regulates the ubiquitin ligase HUWE1. *Elife* 6: e21036

Saunders DN, Hird SL, Withington SL, Dunwoodie SL, Henderson MJ, Biben C, Sutherland RL, Ormandy CJ, Watts CKW (2004) Edd, the murine hyperplastic disc gene, is essential for yolk sac vascularization and chorioallantoic fusion. *Mol Cell Biol* 24: 7225 – 7234

Schukur L, Zimmermann T, Niewoehner O, Kerr G, Gleim S, Bauer-Probst B, Knapp B, Galli GG, Liang X, Mendiola A *et al* (2020) Identification of the HECT E3 ligase UBR5 as a regulator of MYC degradation using a CRISPR/Cas9 screen. *Sci Rep* 10: 20044

Scialpi F, Mellis D, Ditzel M (2015) EDD, a ubiquitin-protein ligase of the N-end rule pathway, associates with spindle assembly checkpoint components and regulates the mitotic response to nocodazole. *J Biol Chem* 290: 12585 – 12594

Shearer RF, Iconomou M, Watts CKW, Saunders DN (2015) Functional roles of the E3 ubiquitin ligase UBR5 in cancer. *Mol Cancer Res* 13: 1523 – 1532

Sherpa D, Chrustowicz J, Qiao S, Langlois CR, Hehl LA, Gottemukkala KV, Hansen FM, Karayel O, von Gronau S, Prabu JR *et al* (2021) GID E3 ligase supramolecular chelate assembly configures multipronged ubiquitin targeting of an oligomeric metabolic enzyme. *Mol Cell* 81: 2445 – 2459

Song M, Wang C, Wang H, Zhang T, Li J, Benezra R, Chouchane L, Sun Y-H, Cui X-G, Ma X (2020a) Targeting ubiquitin protein ligase E3 component N-recognin 5 in cancer cells induces a $CD8^+$ T cell mediated immune response. *Onco Targets Ther* 9: 1746148

Song M, Yeku OO, Rafiq S, Purdon T, Dong X, Zhu L, Zhang T, Wang H, Yu Z, Mai J *et al* (2020b) Tumor derived UBR5 promotes ovarian cancer growth and metastasis through inducing immunosuppressive macrophages. *Nat Commun* 11: 6298

Sonn-Segev A, Belacic K, Bodrug T, Young G, VanderLinden RT, Schulman BA, Schimpf J, Friedrich T, Dip PV, Schwartz TU *et al* (2020) Quantifying the heterogeneity of macromolecular machines by mass photometry. *Nat Commun* 11: 1772

Tasaki T, Zakrzewska A, Dudgeon DD, Jiang Y, Lazo JS, Kwon YT (2009) The substrate recognition domains of the N-end rule pathway. *J Biol Chem* 284: 1884 – 1895

UniProt Consortium (2021) UniProt: the universal protein knowledgebase in 2021. *Nucleic Acids Res* 49: D480 – D489

Varshavsky A (2011) The N-end rule pathway and regulation by proteolysis. *Protein Sci* 20: 1298 – 1345

Verdecia MA, Joazeiro CAP, Wells NJ, Ferrer J-L, Bowman ME, Hunter T, Noel JP (2003) Conformational flexibility underlies ubiquitin ligation mediated by the WWP1 HECT domain E3 ligase. *Mol Cell* 11: 249 – 259

de Vivo A, Sanchez A, Yegres J, Kim J, Emly S, Kee Y (2019) The OTUD5-UBR5 complex regulates FACT-mediated transcription at damaged chromatin. *Nucleic Acids Res* 47: 729 – 746

Wang J, Zhao X, Jin L, Wu G, Yang Y (2017) UBR5 contributes to colorectal cancer progression by destabilizing the tumor suppressor ECRG4. *Dig Dis Sci* 62: 2781 – 2789

Wang F, He Q, Zhan W, Yu Z, Finkin-Groner E, Ma X, Lin G, Li H (2023) Structure of the human UBR5 E3 ubiquitin ligase. *Structure* 31: 541 – 552

Waterhouse AM, Procter JB, Martin DMA, Clamp M, Barton GJ (2009) Jalview Version 2—a multiple sequence alignment editor and analysis workbench. *Bioinformatics* 25: 1189 – 1191

Welcker M, Wang B, Rusnac D-V, Hussaini Y, Swanger J, Zheng N, Clurman BE (2022) Two diphosphorylated degrons control c-Myc degradation by the Fbw7 tumor suppressor. *Sci Adv* 8: eabl7872

Welsh KA, Bolhuis DL, Nederstigt AE, Boyer J, Temple BRS, Bonacci T, Gu L, Ordureau A, Harper JW, Steimel JP *et al* (2022) Functional conservation and divergence of the helix-turn-helix motif of E2 ubiquitin-conjugating enzymes. *EMBO J* 41: e108823

Yamaguchi M, Yu S, Qiao R, Weissmann F, Miller DJ, VanderLinden R, Brown NG, Frye JJ, Peters J-M, Schulman BA (2015) Structure of an APC3–APC16 complex: insights into assembly of the anaphase-promoting complex/cyclosome. *J Mol Biol* 427: 1748 – 1764

Yau RG, Doerner K, Castellanos ER, Haakonsen DL, Werner A, Wang N, Yang XW, Martinez-Martin N, Matsumoto ML, Dixit VM *et al* (2017) Assembly and function of heterotypic ubiquitin chains in cell-cycle and protein quality control. *Cell* 171: 918 – 933

Youkharibache P, Veretnik S, Li Q, Stanek KA, Mura C, Bourne PE (2019) The small β-barrel domain: a survey-based structural analysis. *Structure* 27: 6 – 26

Zhang T, Cronshaw J, Kanu N, Snijders AP, Behrens A (2014) UBR5-mediated ubiquitination of ATMIN is required for ionizing radiation-induced ATM signaling and function. *Proc Natl Acad Sci U S A* 111: 12091 – 12096